

ARTICLE OPEN



Epigenomic mapping identifies an enhancer repertoire that regulates cell identity in bladder cancer through distinct transcription factor networks

Hélène Neyret-Kahn ^{1,2,13,14}✉, Jacqueline Fontugne^{1,3,4,14}, Xiang Yu Meng^{1,2,5}, Clarice S. Groeneveld^{1,2,6}, Luc Cabel ^{1,2}, Tao Ye ⁷, Elodie Guyon^{1,8}, Clémentine Krucker^{1,2,3}, Florent Dufour^{1,2}, Elodie Chapeaublanc ^{1,2}, Audrey Rapinat⁹, Daniel Jeffery¹⁰, Laura Tanguy^{1,2}, Victoria Dixon^{1,3}, Yann Neuzillet^{4,11}, Thierry Lebrét^{4,11}, David Gentien⁹, Irwin Davidson ¹², Yves Allory^{1,3,4}, Isabelle Bernard-Pierrot ^{1,2,15} and François Radvanyi ^{1,2,15}

© The Author(s) 2023

Muscle-invasive bladder cancer (BLCA) is an aggressive disease. Consensus BLCA transcriptomic subtypes have been proposed, with two major Luminal and Basal subgroups, presenting distinct molecular and clinical characteristics. However, how these distinct subtypes are regulated remains unclear. We hypothesized that epigenetic activation of distinct super-enhancers could drive the transcriptional programs of BLCA subtypes. Through integrated RNA-sequencing and epigenomic profiling of histone marks in primary tumours, cancer cell lines, and normal human urothelia, we established the first integrated epigenetic map of BLCA and demonstrated the link between subtype and epigenetic control. We identified the repertoire of activated super-enhancers and highlighted Basal, Luminal and Normal-associated SEs. We revealed super-enhancer-regulated networks of candidate master transcription factors for Luminal and Basal subgroups including FOXA1 and ZBED2, respectively. FOXA1 CRISPR-Cas9 mutation triggered a shift from Luminal to Basal phenotype, confirming its role in Luminal identity regulation and induced ZBED2 overexpression. In parallel, we showed that both FOXA1 and ZBED2 play concordant roles in preventing inflammatory response in cancer cells through STAT2 inhibition. Our study furthers the understanding of epigenetic regulation of muscle-invasive BLCA and identifies a co-regulated network of super-enhancers and associated transcription factors providing potential targets for the treatment of this aggressive disease.

Oncogene (2023) 42:1524–1542; <https://doi.org/10.1038/s41388-023-02662-1>

INTRODUCTION

Bladder cancer is the tenth most common cancer worldwide, accounting for nearly two thousand cancer-related deaths globally in 2018 [1]. Urothelial carcinoma is classified as non-muscle-invasive bladder cancer (NMIBC comprising carcinoma in situ, and the pTa and pT1 stages) or the aggressive muscle-invasive bladder cancer (MIBC, stages pT2 to pT4), depending on the level of invasion into the bladder wall [2]. Molecular classifications of bladder carcinomas have been established using mainly gene expression profiling studies [3–8]. A recent consensus classification of MIBC presents six subtypes, from which tumours can be coarsely divided into two subgroups: the Luminal and the non-Luminal subgroups. Luminal subgroup comprises three Luminal

subtypes (LumU, LumNS and LumP), whereas Basal-Squamous subtype (Ba/Sq) constitutes the major part of the non-luminal subgroup [3]. Luminal tumours, accounting for about 50% of MIBCs, present high expression of urothelial differentiation markers (GATA3, FOXA1, KRT20, uroplakins) and are enriched in activating mutations of *FGFR3* [3]. Basal tumours, also called Basal/Squamous, are particularly aggressive and account for ~35% of MIBCs [3]. They are characterized by the overexpression of markers of the basal layer of the urothelium (including KRT5, KRT6), the under-expression of markers of luminal differentiation and activation of EGFR [9]. Concerning the NMIBC tumours, the recent UROMOL studies group them into 4 classes including Class 1 associated with luminal differentiation and good prognosis, and

¹Molecular Oncology, PSL Research University, CNRS, UMR 144, Institut Curie, Equipe Labellisée Ligue Nationale Contre le Cancer, Paris, France. ²Sorbonne Universités, UPMC Université Paris 06, CNRS, UMR144, 75005 Paris, France. ³Department of Pathology, Institut Curie, Saint-Cloud, France. ⁴Université Versailles St-Quentin, Université Paris-Saclay, F-78180 Montigny-le-Bretonneux, France. ⁵College of Basic Medical Sciences, Medical School, Hubei Minzu University, Enshi 445000, China. ⁶Université de Paris, Centre de Recherche des Cordeliers, Paris, France. ⁷Institut de Génétique et de Biologie Moléculaire et Cellulaire (IGBMC), Institut National de la Santé et de la Recherche Médicale (INSERM) U1258, Centre National de Recherche Scientifique (CNRS) UMR7104, Université de Strasbourg, 1 rue Laurent Fries, 67404 Illkirch, France. ⁸Department of Pathology, Institut Curie, Paris, France. ⁹Department of Translational Research, Genomics Platform, Institut Curie, PSL Research University, Paris, France. ¹⁰Urology Medico-Scientific Program, Department of Translational Research, Institut Curie, PSL Research University, Paris, France. ¹¹Department of Urology, Hôpital Foch, Suresnes, France. ¹²Department of Functional Genomics and Cancer, Institut de Génétique et de Biologie Moléculaire et Cellulaire, CNRS/INSERM/UDS, 67404 Illkirch Cedex, France. ¹³Present address: INSERM U830, Equipe Labellisée LNCC, Diversity and Plasticity of Childhood Tumors Lab, PSL Research University, SIREDO Oncology Center, Institut Curie Research Center, Paris, France. ¹⁴These authors contributed equally: Hélène Neyret-Kahn, Jacqueline Fontugne. ¹⁵These authors jointly supervised this work: Isabelle Bernard-Pierrot, François Radvanyi.

✉email: helene.neyret-kahn@curie.fr

Received: 18 October 2022 Revised: 1 March 2023 Accepted: 6 March 2023

Published online: 22 March 2023

a Class 2a comprising high risk tumours [7, 8]. One hypothesis to explain the establishment of the different subtypes and their potential plasticity, is that each subtype harbours a regulatory network in which various upstream genomic and epigenomic alterations lead to the activation of a core set of master transcription factors (TFs) that then determine a transcriptomic downstream program. While transcriptional regulators of urothelial differentiation, such as FOXA1, GATA3 and PPAR γ , have been established as key regulators of the Luminal phenotypes, the essential transcription regulators driving the Ba/Sq subtype have not been elucidated [10–14].

Recent studies have demonstrated that altered enhancer activity drives changes in cell identity and oncogenic transformation, notably through large clusters of highly active enhancers called super-enhancers (SEs) [15–17]. While the specific functional characteristics of SE are still unclear [18], it has been demonstrated that super-enhancers are more significantly associated with tumor-specific genes and genes playing a prominent role in cell identity [17, 19, 20]. Indeed, targeting SE-driven oncogenesis has become a novel therapeutic approach with the advent of BRD4 inhibitors, which inhibit SE activation [21]. By regulating the expression of a small number of master TFs, SEs can orchestrate cell- or cancer-specific transcriptional programs. H3K27ac enrichment has been widely utilized as a surrogate for identifying SEs [17] and H3K27ac signal and derived SEs have been demonstrated to classify various types of cancer [22–25]. The ENCODE roadmap, that profiled histone marks in normal and cancer cell lines, has become a valuable source of information to uncover chromatin organisation, alteration, and subsequent regulation of master regulators but did not include bladder models [26]. Recently, two studies provided new insights with the profiling of particular histone marks in bladder cancer samples and cell lines [27, 28]. Here, we further characterized bladder cancer epigenetics by integrating transcriptomic and epigenomic profiling of multiple histone marks in human bladder tumours, bladder cancer cell lines, and primary cultures from normal urothelia to produce a comprehensive bladder cancer epigenetic map. With this map, we demonstrated the link between molecular subtype and the underlying epigenetic landscape. Through H3K27ac analysis, we established a repertoire of SEs that are specific to distinct subgroups (Luminal, Ba/Sq subtypes, as well as Normal primary cells), highlighting SE-associated genes with subgroup-specific clinical relevance. From there, we identified the core SE-regulated networks of master TFs that distinguish luminal and basal subgroups, including known and new candidate master TFs. Finally, through functional knock-down and knock-out experiments, we revealed that one of these master TFs (FOXA1) is a key factor in subtype determination antagonized by ZBED2, and that both FOXA1 and ZBED2 present the ability to dampen inflammatory response. Overall, this work provides new data characterizing epigenetic regulation in bladder cancer. We reveal important genes that can be essential for maintenance of bladder cancer cell identity and present potential new targets to treat aggressive bladder cancers.

RESULTS

Integrated bladder cancer chromatin landscape

To elucidate the contribution of chromatin landscape in bladder cancer biology, we generated ChIP-seq for active (H3K27ac) and repressive histone marks (H3K27me3, H3K9me3) in 24 bladder samples (Fig. 1). In order to distinguish features of the non-cancerous stromal cells and of normal urothelial cells, we used not only human primary tumours ($n = 15$) from the CIT (*Carte d'Identité des Tumeurs*) cohort [9, 29], but also cellular models (7 bladder cancer cell lines) and patient-derived Normal Human Urothelium in proliferation (NHU, $n = 2$). Of note, tumours were macrodissected to enrich for bladder cancer content (Figs. 1, S1A). Of the

15 primary tumours, we included 13 MIBCs and 2 NMIBCs to assess the stage-dependence of our results (Figs. 1, S1A, and Table S1). With the aim of identifying subtype-specific epigenetic alterations/characteristics, we coupled our ChIP-seq with RNA-seq from the same extraction and classified them according to the current consensus subtypes [3]. Of the 13 MIBCs, 2 classified as stromal-rich, 5 classified as basal/squamous (Ba/Sq) and 6 as luminal, including 1 luminal papillary (LumP), 3 luminal unstable (LumU) and 2 luminal non-specified (LumNS). Of the 7 cell lines, 3 were classified Ba/Sq, 3 LumP and one could not be classified (Table S1A, B, see methods) [30]. Using the recent UROMOL classifier, the two NMIBC samples classified as class 3 [7, 8]. Further analysis using subtype deconvolution (WISP [31]), and previously described regulatory signatures [3, 7], revealed that one of the tumours originally classified as Ba/Sq (T391) was composed of a mixed population of LumP and Ba/Sq cells (Fig. S1B, C).

We also assessed molecular subtypes using immunohistochemistry (IHC) with luminal (GATA3 and CK20) and basal (CK5/6) markers in our primary tumours ($n = 13$) and bladder cancer cell lines ($n = 7$). We added p16 to distinguish LumU samples from the other luminal subtypes [32]. As expected, the majority of Ba/Sq tumours in the consensus classification scheme showed a typical CK5/6 + /GATA3-/CK20- expression phenotype (Fig. S1D). In contrast, all tumours of Luminal consensus subtypes showed the opposite immunophenotype, and most LumU samples additionally highly expressed p16. Interestingly, the IHC analysis confirmed our subtype deconvolution (WISP) and transcriptomic signature analyses (Fig. S1B, C) by showing a co-expression of luminal and basal markers in T391. Given its mixed phenotype, tumour T391 was excluded from differential analyses between subgroups. Four cell lines showed similar concordant results according to mRNA subtype. Among the 3 remaining cell lines, one Ba/Sq and one LumP consensus subtype cell line showed atypical immunophenotypes, and the non-classified KK47 cell line was negative for all markers but p16 (Fig. S1D).

Peak calling using MACS showed that ChIP-seq for H3K27ac gave the most homogeneous and highest number of peaks across the 24 samples (Fig. S2A–C).

We integrated our multi-factorial ChIP-seq profiles using ChromHMM [33], reporting the first integrated epigenetic map in bladder cancer in both primary tumour samples and cell lines (Fig. 2A). Six chromatin states (E1–E6) were assigned according to histone mark enrichments, as previously described (ENCODE, Roadmap project [26]), where H3K27ac-enriched regions correspond to active promoters and enhancers (E2), H3K27me3 and H3K9me3-enriched states associate with repression (E4) or heterochromatin (E6), and regions enriched in both active and repressive marks define bivalent enhancers or promoters (E3). Regions without any marks or only weak H3K9me3 enrichment were designated as quiescent/no marks (E1) or quiescent/weakly repressed (E5), respectively (Figs. 2A, S3A, B). Analysis of associated RNA-seq data confirmed that gene expression correlates with the expected chromatin states (Figs. 2B, S3C). Briefly, genes with transcription start sites (TSSs) in E2 states (active enhancers / promoters) have the highest expression levels, followed by those in E3 states (bivalent enhancers / promoters). Minimal expression was noted for genes with TSSs in the remaining states.

Chromatin states classify bladder cancers by transcriptomic subgroups

Next, we sought to classify our samples based on chromatin states for comparison with molecular subtypes. To do this we first performed an unsupervised analysis to select the most distinguishing features from the chromatin profiles (see methods, Fig. S3D) and plotted all samples by multiple correspondence analysis on the most varying regions (MCA, Fig. S3E). Similar to Principal Component Analysis (PCA), but adapted for categorical

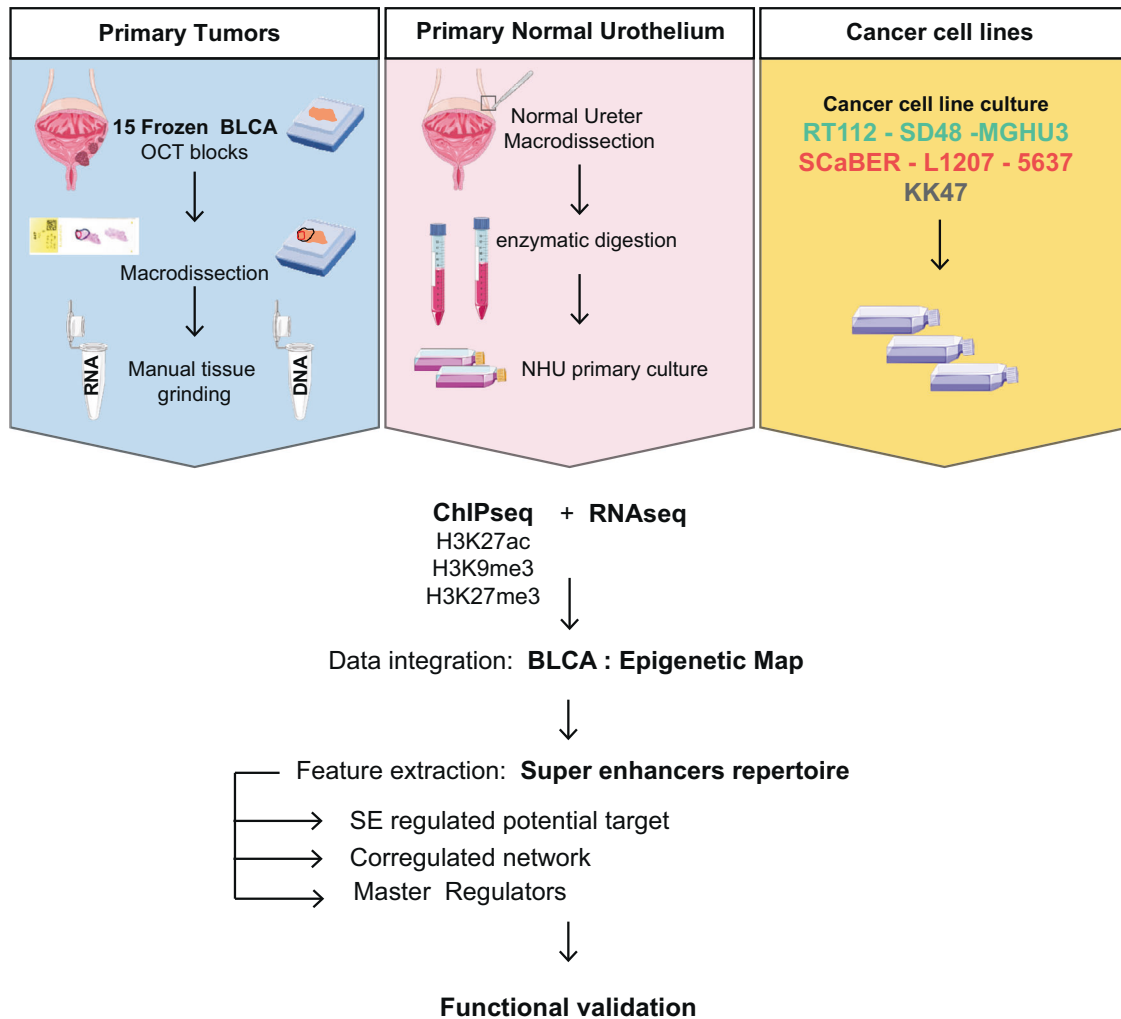


Fig. 1 Methodology/Workflow. Macrodissected BLCA Primary Tumours, Normal Proliferating NHU as well as cell lines were subjected to ChIP-seq for Histone H3K27ac, H3K27me3 and H3K9me3 as well as RNA-seq. Integrated analyses were used to establish an epigenetic map and identify Master regulators of major BLCA subgroups.

data, this method of dimensionality reduction separates samples in 2D space by proximity according to the primary (Dim 1) and secondary (Dim 2) dimensions. Thus, greater differences in chromatin profiles are represented by greater distances in the 2D plot. Dim 1 distinguished primary tumour samples from cell lines, which could be indicative of chromatin changes associated with cell culture or stroma content. Interestingly, Dim 2 distinguished Non-basal from Basal subgroups. To confirm this distinction of molecular subtypes, we re-assessed the data with an alternative dimensionality reduction method (MDS), coupled to a batch effect-like correction (MNN), which eliminated most of the cell line vs primary tumour differences while maintaining and strengthening the distinction between Non-Basal and Basal subgroups along Dim 2 (Fig. 2C). Therefore, we identified two clusters derived from differences in chromatin state that are associated with molecular subtypes; a “basal cluster” containing all Ba/Sq samples (except the mixed T391), and a “non-basal cluster” including all luminal, stroma-rich and NMIBC samples (Fig. 2C). Interestingly, NHU cells were located at the border between the two groups (Fig. 2C). To explore the biological pathways associated with the chromatin profiles that could distinguish Luminal from Basal bladder cancers, we ranked genes based on the MCA outputs for Dim 2 and performed Gene Set Enrichment Analysis (GSEA [34, 35], Fig. 2D). As expected, for the basal cluster, we found that active chromatin (E2) was strongly enriched at

genes involved in decreased Luminal differentiation, while repressive chromatin (E4) was strongly depleted for these genes (Fig. 2D). Interestingly, genes involved in increased tumour aggressiveness, stemness, extracellular matrix, epithelial-mesenchymal transition and invasion were also enriched in active chromatin and depleted for repressive chromatin in the basal cluster (Fig. 2D). Taking an alternative approach, we derived Basal and Luminal gene signatures from an independent publicly available scRNA-seq dataset (GSM4307111 [36]) and compared these genes with the chromatin states associated with the basal and non-basal clusters identified in Fig. 2C (Fig. 2E, see methods). Luminal signature genes were enriched in active state in the non-basal chromatin cluster while Basal signature genes were enriched in active state in the basal chromatin cluster, suggesting epigenetic regulation of signature genes involved in urothelial differentiation. We further illustrate this relationship with two well-described example markers of bladder cancer subtypes: *FOXA1* and *KRT6A* (Fig. 2F). *FOXA1* expression is higher in Luminal than Basal tumours [9, 11, 14, 37–40]. In agreement, our results showed that *FOXA1* was marked with active (E2) chromatin in most Luminals (including LumP, LumNS and LumU), NMIBC samples, and even NHU cells. Interestingly, 3 out of 4 Ba/Sq primary tumors harbored repressive chromatin (E4), suggesting polycomb-mediated repression (Fig. 2F). Active enhancer regions upstream of *FOXA1* gene, inside *MIPOL1* gene, appeared specifically active in

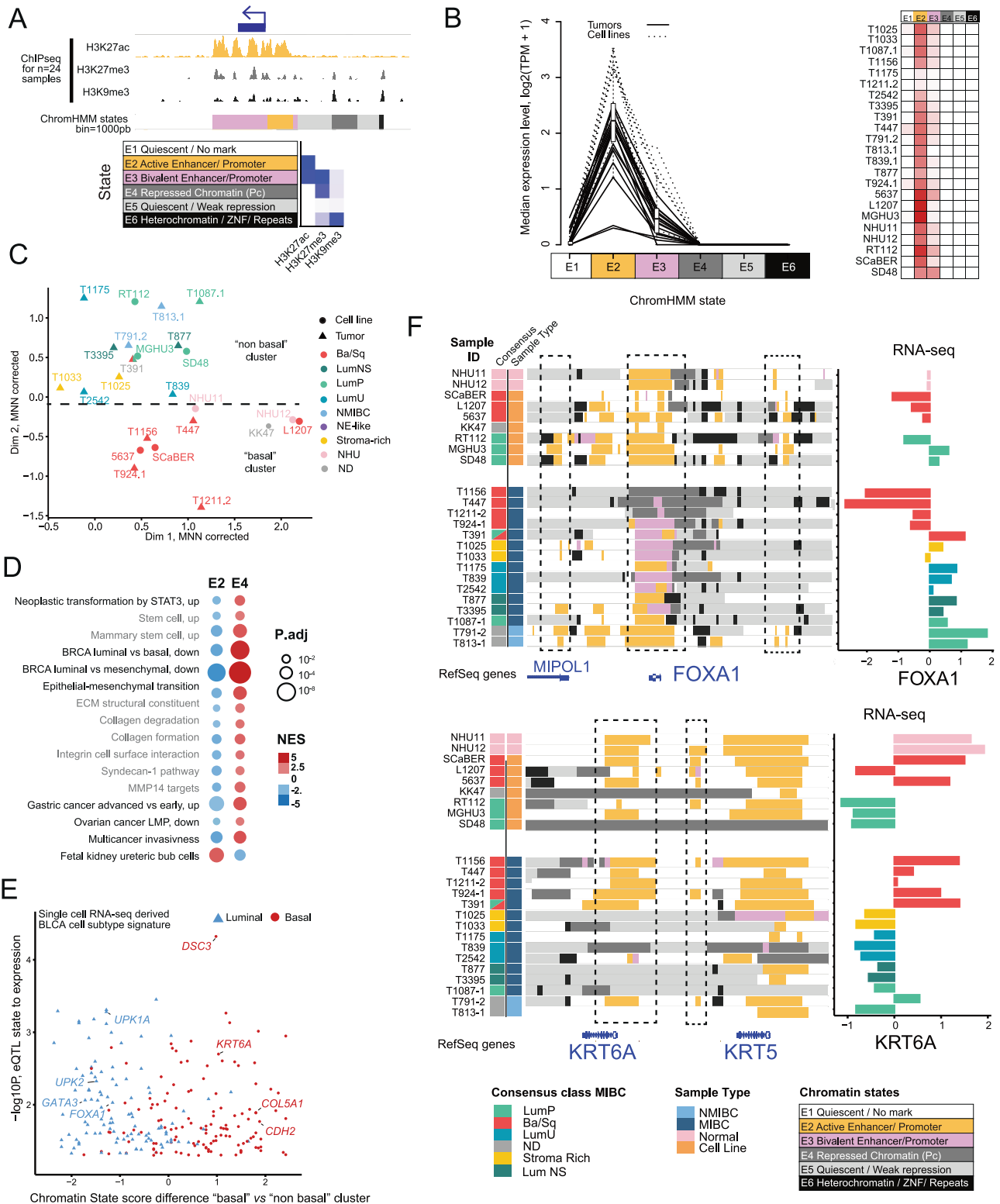


Fig. 2 Chromatin states classify bladder cancers by subgroups. **A** ChromHMM principle example and emission order dividing genome in 6 states based on combination of H3K27ac, H3K27me3 and H3K9me3 marks. **B** Gene-expression level by chromatin state at transcription start site. **C** Two chromatin state clusters revealed by unsupervised analysis of top 1% varying regions using MDS for dimension reduction plus MNN for batch effect correction. **D** GSEA functional enrichment analysis of the genes mapped to the MCA Dim2 contributing features. A negative NES indicates significant enrichment in lower Dim2 coordinates (Basal direction), and the reverse is in higher Dim2 coordinates (Luminal direction). **E** Luminal versus basal tumour cell signature genes identified with single cell RNA-seq analysis showing concordant enrichment in chromatin state clusters. **F** Genome Browser view of chromatin states at *FOXA1* and *KRT6* loci with corresponding RNA-seq (VST normalized scaled expression). Regulatory regions of interest are highlighted with dashed-line rectangles.

NMIBC and Luminal samples, correlating with *FOXA1* expression level (Fig. 2F). On the other hand, *KRT6A*, commonly expressed in Basal tumours [3], had active chromatin marks in seven out of eight Ba/Sq samples, as well as NHU, whereas most luminal samples showed no mark or quiescent/weak repression states. Taken together, these results demonstrate the importance of both active and repressive histone marks in the regulation of gene expression driving cell identity in bladder cancer.

Identification of the bladder enhancer repertoire and subtype specificities

To determine if chromatin profiles identify enhancers that could control bladder cancer subtype, we determined and annotated enhancer and particularly large clusters of enhancers. We applied the ROSE algorithm (Table S2), which calls and stitches enhancers in close proximity (using the 12.5 kb default parameter), then ranks enhancers according to H3K27ac signal. These large clusters of stitched enhancers (mean size = 101 967 pb) were hereafter termed *super-enhancers*, a terminology initially defined by the developers of the algorithm [21, 41]. Despite signal correction using input, the number of called SEs by ROSE was notably lower in samples with gene amplifications, owing to very high H3K27ac signal in amplified regions, thus creating a bias in the ranked enhancer plot (Fig. S4A, B). To correct for the copy-number bias, we adapted the final step of the ROSE pipeline, as previously described by Aldiri et al. [42], setting a threshold and defining the top 1000 ranked ROSE enhancer regions in each sample as SEs for all downstream analyses, approximately representing the mean number of ROSE SEs per sample (mean = 956 SEs, Table S2, Fig. S4C) [42].

To gain insight into subtype-specific enhancer alterations and assess sample similarity based on these SE profiles, we determined the global repertoire of SEs in bladder by extracting a consensus set of SEs. The number of consensus SE highly varied when filtering SE regions detected in a minimum of samples (Fig. S4D). Therefore, to avoid potential artefacts driven by only one sample, we focused on 2887 consensus SEs present in at least 2 of our 24 samples (Table S3). Using PCA of H3K27ac signal corresponding only to the consensus SE regions, we again found that samples were grouped according to molecular subgroup, separating Basals from Luminals, NMIBC segregating with differentiated tumours and NHU with Basal cells as a reflection of their dedifferentiated and proliferative state (Fig. 3A). This reveals that the variability in SE profiles reflects the differences in Basal and Luminal transcriptional programs. The same PCA performed on the unfiltered 4313 SE set show a very similar pattern, revealing that our filtering retained the major SE contributing to subtype differences (Fig. S4E).

We sought to further explore the functional pathway enrichment of SE-regulated genes. We first assigned SEs to their closest and most transcriptionally correlated genes (see methods). For example, a large SE mapped close to *KLF5*, whose expression was correlated with SE activity mostly in Luminal samples, as previously reported [43] (Fig. 3B). In contrast, *KLF7* was regulated by a SE mostly active in Basal samples (Fig. 3B). We then performed pairwise differential analyses between subtypes (Figs. 3C, S3E). The comparison between Basal and Luminal samples identified 379 subgroup-specific SEs (Fig. 3C, Table S3). By comparing the differential SEs to RNA-seq differential expression analysis, we confirmed that luminal-gained SEs showed significantly higher activation levels in Luminal samples relative to Basal samples and vice-versa for basal-gained SEs (Fig. 3D). We then validated the subgroup-specific SE-associated genes identified in our samples in a larger dataset, leveraging the gene expression profiles of the TCGA-BLCA MIBC cohort across molecular subtypes ($n = 406$) [40, 44]. Hierarchical clustering of TCGA samples using the genes associated to the most differentially regulated SEs in our consensus repertoire recovered the molecular classification

(Fig. S4F, Table S3). Strikingly, differential analysis between Basal and Luminal SEs revealed that Luminal-specific SEs were attributed to known transcriptional drivers of the luminal phenotype, namely *GATA3*, *PPARG*, *FOXA1* [14, 29]. Luminal-gained SEs were associated with “Signaling by TGF-beta family members”, notably due to SEs annotated close to negative regulators of TGF-beta signaling such as the E3 Ubiquitin ligase *SMURF1* or *SMAD6* (Fig. 3C, E, Table S4). In contrast, SE regions significantly bound at higher levels in the Basal tumours were associated with genes known to contribute to Basal cancer biology such as *EGFR*, but also less characterized genes with regards to bladder cancer biology, such as genes related to inflammation and FOXO signaling (*IL7R*, *FBXO32*), signaling by Interleukin or signaling by MET, the activation of which is often correlated with BLCA progression [45] (Fig. 3E). We also identified genes encoding membrane receptors (*IL7R*, *OSMR*, *EGFR*) and transcriptional regulators (*BNC2*, *BNC1*, *HMG2*, *KLF7*, *NR3C1*) as enriched in Basal tumours (Fig. 3C, Table S3). Taking advantage of the NHU samples in our cohort, we extracted differential SEs in three comparisons (Ba/Sq vs NHU vs Luminals, Figs. S4E, 3F, Table S3). This analysis validated the identification of genes that could be specific to cancer biology, such as *IL7R*, *JUN*, *NR3C1* in Ba/Sq subtype, *NPAS2*, *FOXQ1*, *GRHL3* in Luminal samples, or *CDKN2C*, *FOXJ1*, *MEIS2*, *FGFR3* in both subtypes (Fig. 3F, Table S3). Overall, we established a first SE repertoire for bladder cancer, highlighting subgroup-specific, cancer-specific SE activation coupled with gene expression.

Super-enhancers regulate a network of candidate master transcription factors for bladder cancer subgroups

SEs often regulate the expression of master TFs, forming autoregulatory loops and correlated networks [46, 47]. Having established the SE landscape in bladder cancer, we next sought to determine which master regulators control the subtype-specific transcriptional programs. To this end, we overlaid the genomic coordinates of subgroup-specific peaks inside SEs with publicly available ChIP-seq datasets [48, 49]. Our analysis revealed that Luminal-specific SEs were significantly enriched in several TF binding sites (Fig. 4A, Table S5), including known regulators of Luminal subtypes *FOXA1*, *GATA3*, and *ESR1* [3, 14, 40]. Basal-specific SEs were enriched in binding sites of a different set of regulators, including components of the AP-1 complex (*FOSL1*, *FOSL2*, *JUND*, *JUNB*), as well as *SMAD2/3*, *NFKB*, and *STAT3*. Further DNA motif enrichment analysis comparing Basal differential peaks inside subgroup-specific SEs over Luminal ones, again identified AP-1 as a potential regulator of Basal enhancers, as well as *FOXA1*, *FOXA1:AR*, *GATA*, and *GRHL1/2/3* for Luminal enhancers (Fig. 4B, Table S5, Homer [50]).

However, motif binding and ChIP-seq data are not available for all known TFs. To overcome this issue, we designed a method to identify subgroup-associated TFs and their co-regulated networks based on our differential SEs and the large transcriptomic cohort from the TCGA [40] (Fig. 4C). We selected TFs that were regulated by differential SEs (Basal vs Luminal), according to annotations from Lambert et al. [51], and that were differentially expressed in TCGA Ba/Sq vs Luminal subgroups. To identify and evaluate the regulons (group of genes regulated in response to one transcriptional regulator) of the 75 resulting TFs, we inferred the protein activity of these selected TFs using the VIPER algorithm [52]. VIPER infers the protein activity score for each TF based on the expression of a set of genes/targets that are most directly regulated by the given TF, which was obtained from the gene regulatory network inferred by the ARACNe-AP algorithm on the TCGA-BLCA expression dataset [53]. Hierarchical clustering of the resulting TF regulons clustered scores into three groups, which were respectively associated with Luminal, Ba/Sq or Stroma-Rich subtypes (Fig. 4D, E). Since master TFs form interconnected networks with highly correlated levels of expression, we selected

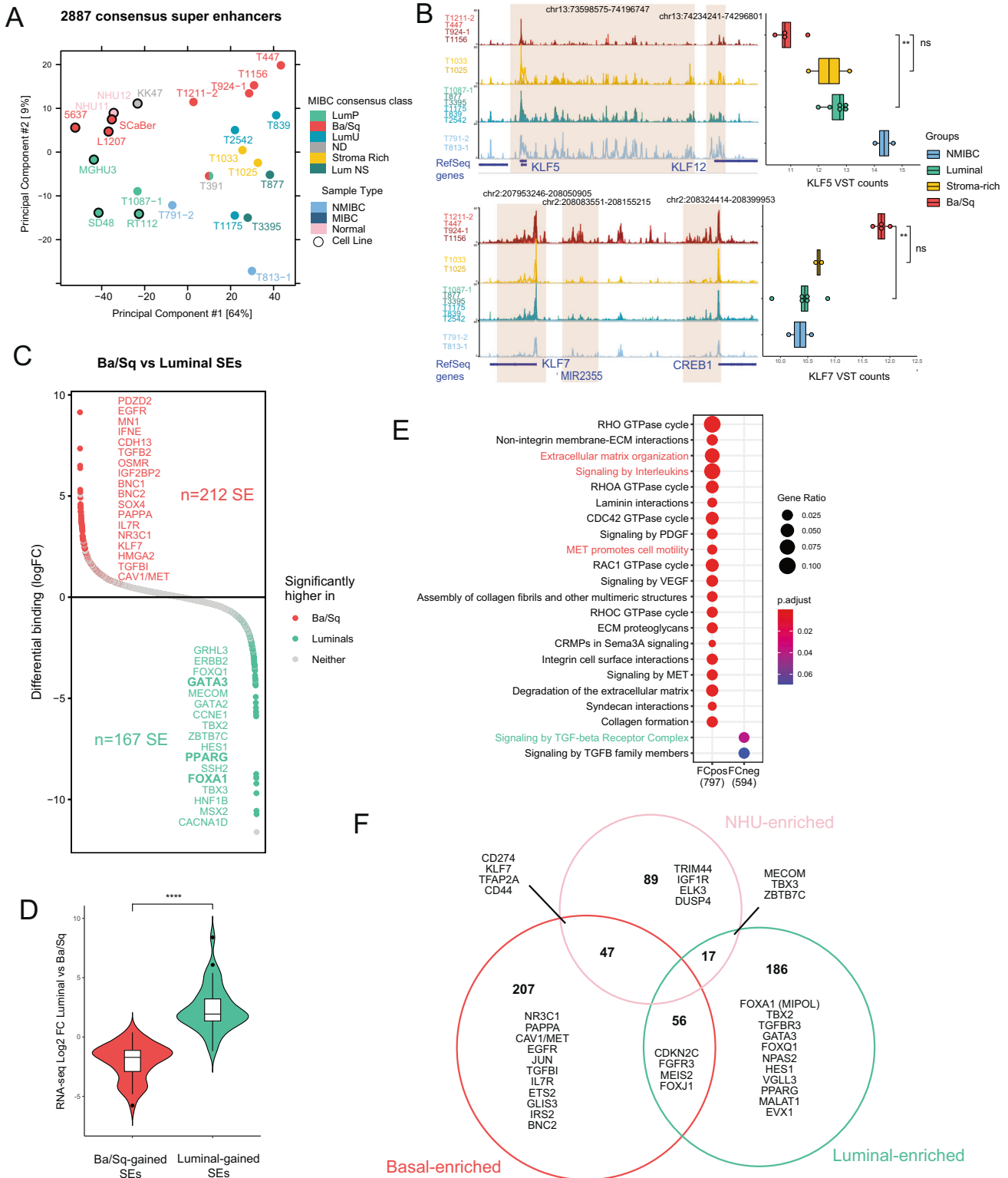


Fig. 3 Identification of the bladder enhancer repertoire and subtype specificities. **A** PCA of H3K27ac signal inside ROSE consensus SE ($n=2887$) for all samples. **B** Representative examples of H3K27ac signal in Ba/Sq, Stroma-Rich, Luminal and NMIBC Tumours with corresponding RNA-seq gene expression. Orange boxes represent SE localisation. **C** Fold Change plots for differentially bound SEs between Ba/Sq and Luminal samples. Significance by p -value < 0.05 . **D** Plot comparing expression LogFC between Ba/Sq and Luminal samples for genes assigned to subgroup-enriched SE. **E** Reactome pathway enrichment analysis of genes associated with Ba/Sq vs Luminal SEs. **F** Venn diagram comparing 3 differential analyses of SE. NHU-enriched SEs are enriched in NHU vs Luminal or NHU vs Basal (pink circle). Basal-enriched SEs are enriched in Basal vs NHU or Basal vs Luminal (red circle). Luminal-enriched SEs are enriched in Luminal vs NHU or Luminal vs Basal (green circle).

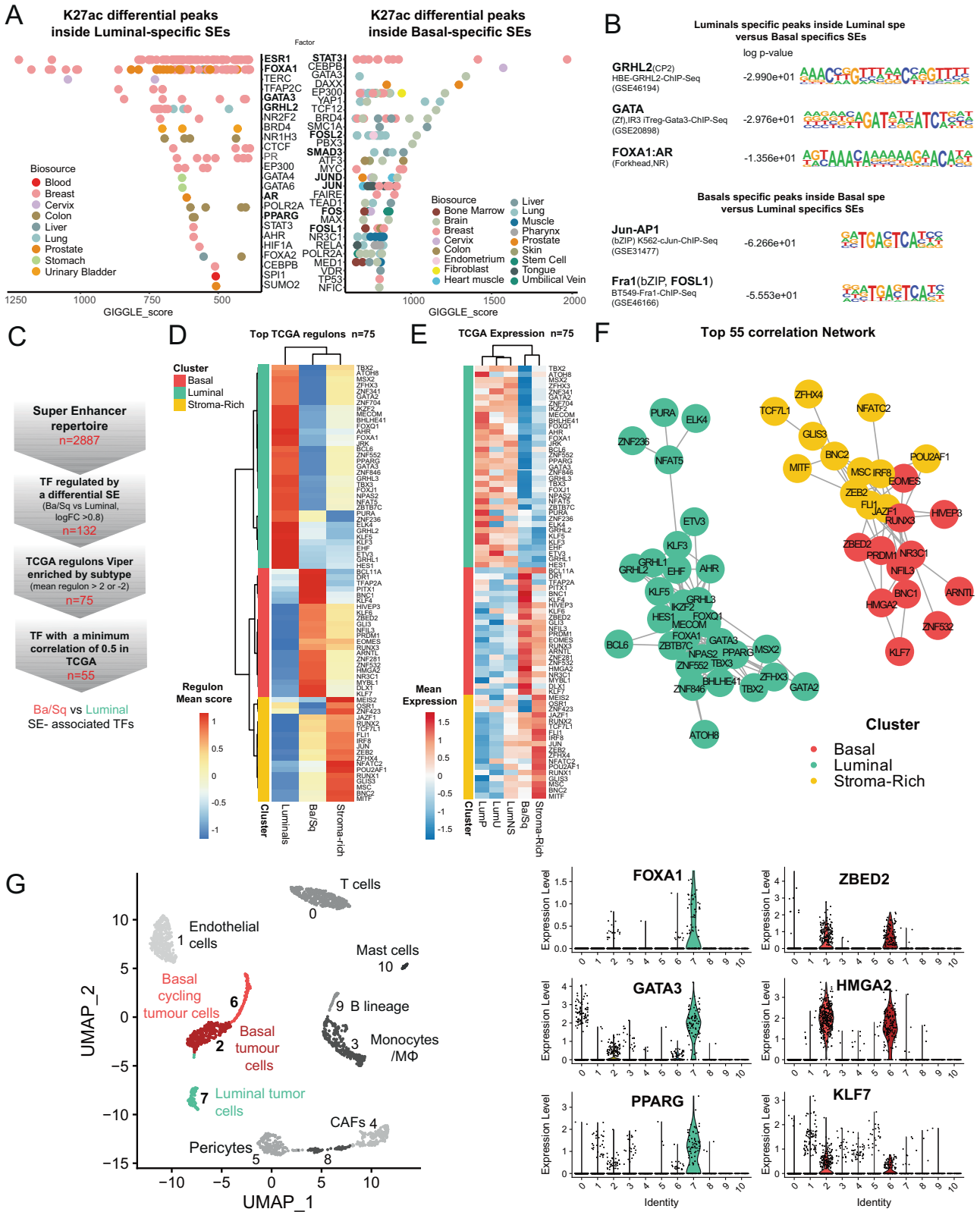


Fig. 4 Super-enhancers regulate a network of candidate master transcription factors for bladder cancer subgroups. A Cistrome analysis of LumP and Ba/Sq specific enhancers. **B** Homer motif enrichment analysis in H3K27ac differential peaks inside differential SE in Luminal vs Basal and Basal vs Luminal. **C** Methodology to identify key coregulated SE-associated TFs. **D** Heatmap of the top 75 TFs with high regulon score. Clustering identified 3 major clusters. **E** Heatmap of the top 75 TFs expression in TCGA-BLCA. **F** Correlation network of the top 55 TFs with an expression correlation coefficient of min 0.5 in TCGA-BLCA cohort. **G** Single-cell RNA-seq analysis of one bladder cancer tumour with both basal and luminal population (GSM4307111 [36]) Right panel, associated expression for key TFs in each compartment.

only TFs whose expression was correlated with that of at least one of the other TFs in TCGA-BLCA data (Pearson correlation coefficient ≥ 0.5 , $n = 55$), and built the top correlated network based on subtype-specific SE-associated TFs (Fig. 4F) (see methods). This strategy identified a large module of Luminal TFs, including known Luminal-associated TFs (e.g., FOXA1/GATA3/PPARG), as well as TFs with yet unexplored roles in Luminal bladder cancer biology (e.g., HES1, FOXQ1, ZBTB7C, MECOM, GRHL2/3, and TBX3). Unlike for Luminals, few TFs have been characterized as key regulators of Basal tumours. Our analysis revealed a network of TFs whose activity could be essential to Basal bladder cancer biology, including HMGA2, KLF7, NR3C1 and ZBED2. Notably, ZBED2 has recently been associated with basal identity in keratinocytes [54] and regulation of inflammation in pancreatic cancer [55].

Combining analyses of tumour and cell line SEs should avoid the identification of master TFs expressed by the stroma. In fact, we found that TFs associated with the Luminal network showed strong expression correlation in our dataset, TCGA-BLCA and in CCLE bladder cell cohorts [56] (Fig. S5A–C) while expression correlations of Stroma-Rich or Basal-associated TFs (e.g., ZEB1, SPI1) were lower for urothelial cell lines in the CCLE [57] compared to those found in primary tumours (Fig. S5A–C). This indicates that expression of those TFs could be dependent on growing conditions and/or interactions with the tumour microenvironment.

To validate our Luminal- and Basal-specific TF networks, we analyzed public single-cell RNA-seq data of a tumour presenting both a Luminal and a Basal cell population (GSM4307111 [36], Fig. S5C). The Luminal-associated TFs FOXA1, GATA3 and PPARG were mostly expressed in the Luminal cell cluster, whereas ZBED2, HMGA2, and KLF7, newly identified as part of the Basal TF network, were mostly expressed in the Basal cell clusters (Fig. 4G), validating our subgroup-specific networks. Together, these analyses identified a targeted subset of interconnected candidate master TFs that could represent key regulators of bladder cancer subgroup identity.

FOXA1 binds subgroup-specific bladder super-enhancers and correlates with their activation

We identified FOXA1 as one of our candidate master TFs for the Luminal bladder cancer subgroup. FOXA1 has been shown to interact with enhancers as a pioneer factor [58] and has a demonstrated impact on Luminal bladder cancer biology [5, 14, 27, 38, 40], though the mechanism for how FOXA1 regulates cell identity is unknown. To better assess the role of FOXA1 in the regulation of bladder cancer SEs, we mapped FOXA1, CTCF (Insulator/enhancers) and H3K4me3 (Promoter) binding by ChIP-seq in two bladder cancer cell lines: SD48 (LumP) and 5637 (Ba/Sq) (Fig. S6A). FOXA1 binding was mostly found outside promoters (Fig. S6B, C), with 61,083 FOXA1 peaks detected in SD48 cells and 39,445 in 5637, an expected variation as FOXA1 was more abundant in Luminal cells (Fig. S6A–C). Despite such differences, we identified three classes of FOXA1 peaks: SD48-specific peaks, peaks overlapping in the two cell lines, and 5637-specific peaks (Figs. 5A, S6D), which suggests that FOXA1 has specific targets in each cell line and subtype. Interestingly, when analysing TF binding sites from publicly available ChIP-seq data, SD48-specific FOXA1 peaks were highly enriched not only for FOXA1 binding sites, but also GATA3 binding sites (Fig. 5B), which could indicate a functional partnership between FOXA1 and GATA3 for regulation of the Luminal program, as suggested by Warrick et al. and described in breast cancer [14, 59]. Surprisingly, 5637-specific FOXA1 peaks were mostly enriched at AP-1 binding sites and not FOXA1 sites (Figs. 5B, S6D). Both enrichments were confirmed by Homer motif analysis of SD48-specific peaks versus 5637-specific peaks or vice versa (Fig. S6E, F [50]). Ontology comparison of genes associated with the three classes of FOXA1 peaks showed that 5637-specific peaks were enriched in terms

associated with Ba/Sq super-enhancers (e.g. Signaling by Tyrosine Kinase, Signaling by MET, Signaling by Interleukin), indicating that FOXA1 might be involved in the regulation of both Luminal and Basal bladder cancer subtypes (Fig. 5C). Indeed, FOXA1 binding in the two cell lines overlapped with most (87%) of the total repertoire of bladder SEs (Fig. 5D) and correlated strongly with H3K27ac levels at these loci (Fig. 5E, F), in line with a role for its regulation of these SEs. Notably, FOXA1 bound at SEs associated with genes involved in regulating urothelial differentiation and strongly correlated with increased H3K27ac at these loci. This could clearly be observed for the Luminal-specific SEs associated with GATA3 or PPARG in the Luminal SD48 cells and in both cell lines for the non-specific PPARG SE. But we also found FOXA1 binding associated with high H3K27ac at certain Basal-specific SEs in the Basal 5637 cells, such as TGF β 2 (Fig. 5G). This implies that FOXA1, even if expressed at a low level as in Ba/Sq cells, could play an important role in BLCA biology, through enhancer/SE regulation. In summary, FOXA1 may regulate bladder cell identity through binding of subgroup-specific bladder enhancers with partners such as GATA3 in Luminal cells and AP-1 in Basal cells.

FOXA1 regulates inflammation and cellular identity

To better understand FOXA1 function, we performed short-term (<72 h) knock-down in both Luminal and Basal models. Knock-down of FOXA1 by siRNA decreased clonogenicity and proliferation of both Luminal and Basal cells (Fig. S7A, B) and it reduced cell viability in both RT112 (LumP subtype) and SCaBER (Ba/Sq) cells, with a stronger impact in RT112 (Fig. 6A). Furthermore, FOXA1 knock-down in RT112 and SCaBER cell lines dramatically altered gene expression (Fig. 6B, Table S6, Fig. S7C). The downregulated genes were related to cell cycle and checkpoint pathways, consistent with the reductions in viability and proliferation upon FOXA1 knock-down. Surprisingly, the upregulated genes in both cell lines were strongly associated with inflammatory signaling and interferon response (Figs. 6C, S7D). Notably, FOXA1 knock-down induced upregulation of master interferon response TFs, STAT1 and STAT2, and key genes involved in the regulation of inflammation in human cancer, including the immune checkpoint modulator CD274 (PD-L1) (Fig. 6D), which we also identified as a downregulated SE in both Luminal and Basal vs NHU cells (see earlier Fig. 3F). While our FOXA1 ChIP-seq in Luminal and Basal cell lines showed FOXA1 binding at many interferon responsive genes, we observed a moderate enrichment on STAT1, STAT2 or CD274 promoters or enhancers and the FOXA1 peaks detected around those genes did not correlate with their expression changes (Fig. S7E). This suggests that the upregulation of these genes upon FOXA1 knock-down is independent of FOXA1 binding of their regulatory elements, in agreement with recent work showing that FOXA1 directly binds and inhibits the STAT2 protein to dampen inflammation in a chromatin-independent manner [60]. Interestingly, if FOXA1 knock down triggered interferon response in both Luminal and Basal models, its depletion affected the Luminal network of co-regulated TFs only in RT112 cells and not in SCaBER (Fig. 6E). PCA projection of TCGA-BLCA transcriptomes together with that of our knock down cells on our scRNA-seq-derived Basal/Luminal signature space confirmed that FOXA1 acute depletion induced a small but consistent shift from Luminal towards Basal subtype only in RT112 cells (Fig. S7F, see methods). Therefore, in agreement with a previous study [14], short-term knock-down of FOXA1 showed a consistent but mild impact on cell identity, not sufficient to majorly alter the subtype of the luminal cells.

Altering the epigenetic landscape could indeed take a longer time. To determine if FOXA1, through its binding to the SE repertoire, regulates the bladder cancer epigenetic landscape and subsequently cellular identity, we produced FOXA1 CRISPR mutant clones allowing long-term FOXA1 inactivation in two Luminal cell lines (SD48 and RT112, Fig. S7G). Despite fundamental differences

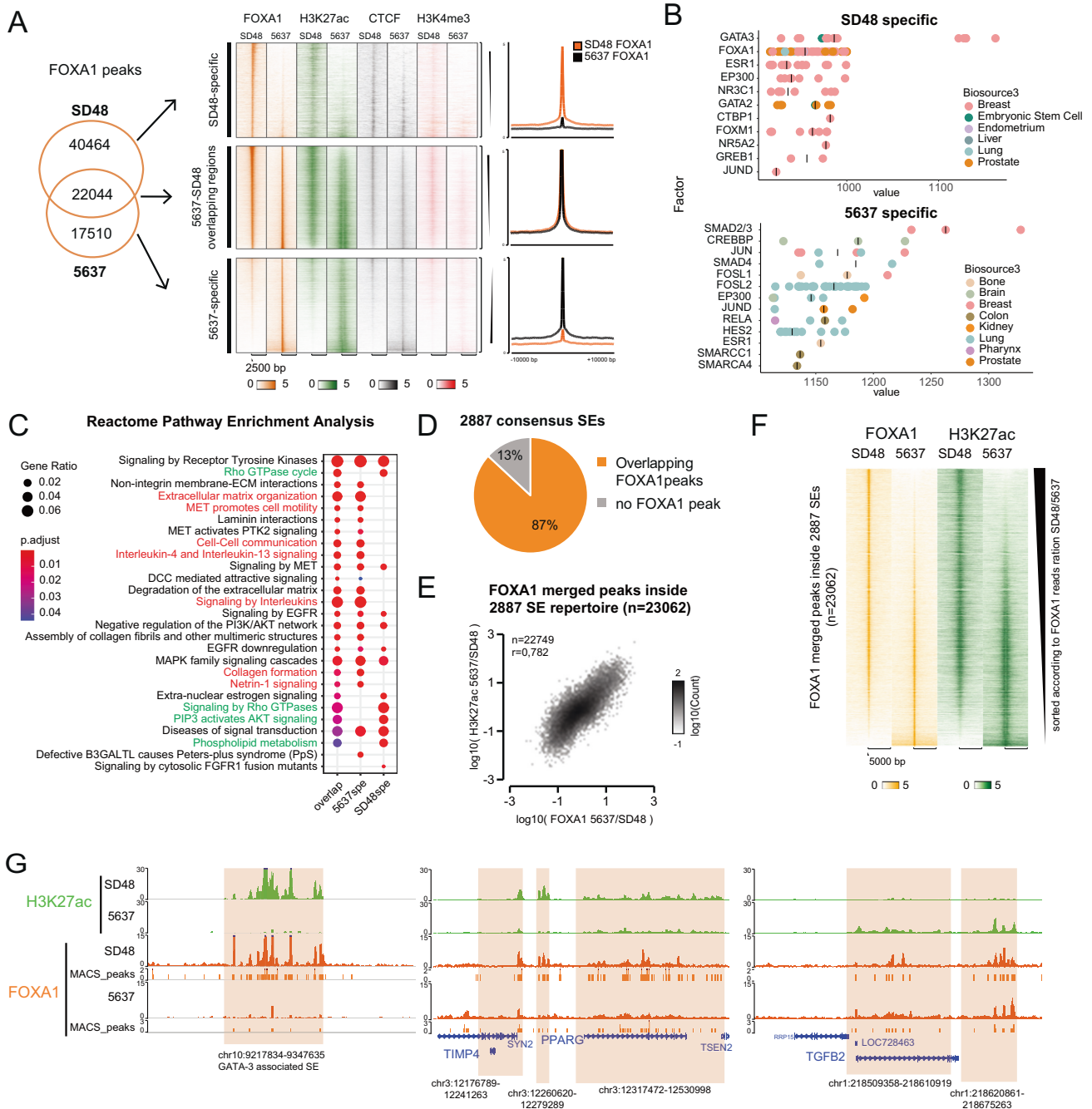
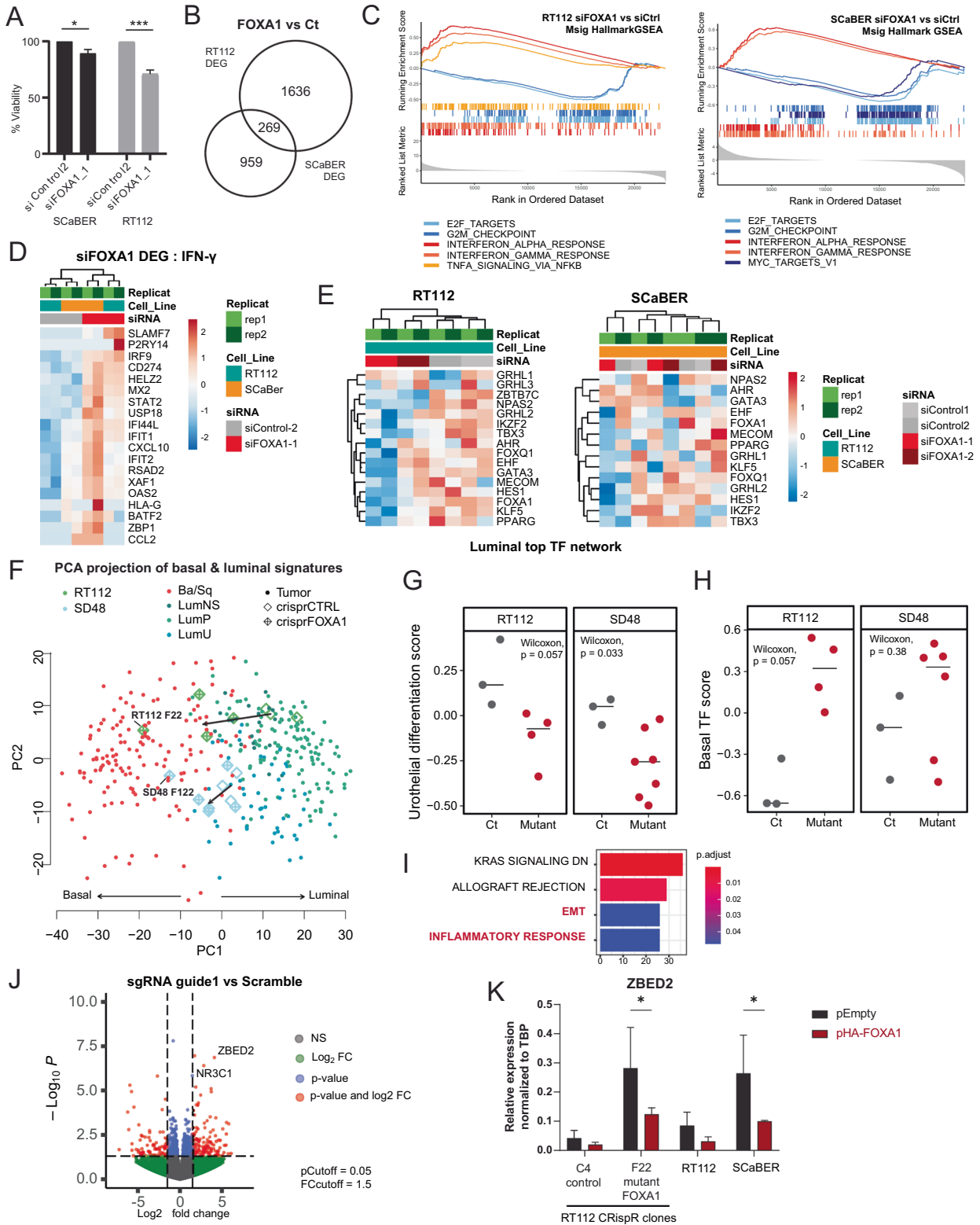


Fig. 5 FOXA1 binds subgroup-specific bladder super-enhancers and correlates with their activation. **A** Venn diagram comparing FOXA1 ChIP-seq peaks in SD48 and 5637 cell line. Heatmap for 3 categories of peaks and associated mean profiles. **B** Cistrome analysis of motif enrichment analysis in SD48-specific and 5637-specific FOXA1 peaks. **C** Reactome pathway analysis of genes associated to the 3 categories of FOXA1 peaks. **D** Pie chart showing proportion of SEs with an overlapping FOXA1 peak (merge of FOXA1 peaks in SD48 and 5637). **E** Correlation between H3K27ac peaks versus FOXA1 peaks inside SEs. **F** Heatmap of FOXA1 and H3K27ac reads on FOXA1 peaks overlapping 2887 SEs ranked by FOXA1 reads ration in SD48 vs 5637. **G** Genome browser view of GATA3, PPARg and TGFB2 associated SEs highlighted with orange boxes.

between RT112 and SD48 cellular models and heterogeneity between clones due to clonal selection, transcriptomic analysis of 3' RNA-seq data by PCA distinguished CRISPR FOXA1 mutant clones from wildtype (WT) (Fig. S6H). Importantly, PCA projection of TCGA-BLCA transcriptomes together with that of our WT and mutant clones on the Basal/Luminal signature space showed that mutation of FOXA1 induced a strong shift from the Luminal cluster to the Basal cluster (Fig. 6F). GSEA analysis confirmed that FOXA1 mutants were enriched for our Basal signature and depleted for

our Luminal signature (Fig. S7I) [34, 35]. GSVA analysis further revealed that FOXA1 mutant clones were less differentiated than WT controls (Fig. 6G [11]) and tended to express higher levels of TFs associated with the Basal TF network (Figs. 6H, 4F). Differential gene expression analysis revealed 1040 and 1102 Differentially Expressed Genes (DEGs) in RT112 and SD48, respectively, when comparing FOXA1 mutant clones to WT (Fig. S7J). FOXA1 mutant DEGs were associated with EMT, KRAS signaling and the inflammatory response pathway (Fig. 6I), all linked to Basal



phenotypes. Intriguingly, differential analysis of *FOXA1* mutants vs WT revealed increased expression of NR3C1 and ZBED2 in the mutants, two of the candidate master TFs identified in our Basal TF network (Fig. 6J, Table S7). Rescue experiment by transient overexpression of HA-FOXA1 in selected CRISPR mutant clones, as well as overexpression in wild-type RT112 and SCaBER, inhibited ZBED2 expression (Figs. 6K, S6K). In summary, our results

demonstrate that loss of *FOXA1* promotes a clear shift from Luminal to Basal cell identity.

ZBED2, a novel Basal-associated TF involved in inflammation dampening

To further explore the interconnected network of candidate master TFs, we chose to examine ZBED2 as one of the TFs in the

Fig. 6 FOXA1 regulates inflammation and cellular identity. **A** Cell viability in RT112 and SCaBER under siRNA treatment against FOXA1. **B** Venn diagram comparing differentially expressed genes in RT112 and SCaBER FOXA1 KD. **C** GSEA plot of Msig Hallmark GSEA Analysis of genes differentially regulated in RT112 and SCaBER cell lines upon FOXA1 siRNA (2 independent siRNA, 2 replicates). **D** Heatmap of genes in Hallmark interferon gamma response genes that are differentially regulated in FOXA1 KD vs Ct (min Fold Change = 1,5). **E** Heatmap of Top Luminal TFs expression in RT112 and SCaBER cell lines upon FOXA1 KD. **F** PCA projection of TCGA Tumours and CRispR mutant clones on the Basal/Luminal signatures. **G** GSEA analysis of FOXA1 CRispR mutant clones on Urothelial differentiation signature from Eriksson et al. **H** GSEA analysis of FOXA1 CRispR mutant clones on Basal TFs identified in Fig. 4F. **I** Overrepresentation analysis of DEG in FOXA1 mutant vs Controls. **J** Volcano plot of Deseq2 RNA-seq analysis comparing pooled CRispR mutant FOXA1 clones in SD48 and RT112 versus controls. **K** Transient overexpression of HA-FOXA1 in mutant FOXA1 CRispR clones, wildtype RT112 and SCaBER. qPCR expression of ZBED2 after transfection of HA-FOXA1 relative to control plasmid, 4 days post transfection including 24 h of Puromycin selection ($n = 3$ for CRispR clones, $n = 2$ for WT RT112 and SCaBER). Significance was calculated using 2way ANOVA test (p -value $< 0.05 = *$).

Basal network since it was upregulated by *FOXA1* CRispR inactivation, and because of recent work in keratinocytes that identified a role for ZBED2 in the basal phenotype [54]. ZBED2 expression in the TCGA-BLCA cohort is upregulated in the Ba/Sq subtype (Fig. 7A) and correlates with poor survival prognosis (Fig. S8A). ZBED2 expression is negatively correlated with FOXA1 expression in the TCGA cohort (Fig. 7B), but more interestingly scRNA-seq in CCLE bladder cell lines shows that FOXA1 and ZBED2 expression are often mutually exclusive (Fig. 7C). As little is known about the ZBED2 TF, we used ARACNE/VIPER algorithms to identify the ZBED2 regulon based on TCGA-BLCA expression data. Interestingly, FOXA1 was predicted as a ZBED2 target, with the most negative weight, whereas two genes associated with Basal-specific SEs (*IL7R* and *CAV1*) were in the top 10 positive ZBED2 regulon weights (Fig. S8B). Using ZBED2 ChIP-seq data from pancreatic cancer cell lines [55] (the only ZBED2 ChIP-seq reported so far), we found a high confidence ZBED2 peak in the *FOXA1* promoter (Fig. 7D, left). Analysis of the RNA-seq data from the same study revealed that ZBED2 overexpression triggered downregulation of FOXA1 (Fig. S8C, $p = 0.004$). In our data, we found that the ZBED2 SE was highly enriched in FOXA1 binding in SD48 luminal cells, whereas FOXA1 binding was significantly decreased in 5637 Ba/Sq cells, and negatively correlated with ZBED2 expression (Fig. 7D, right). Overall, these findings suggest that FOXA1 and ZBED2 could negatively regulate each other to promote or maintain Luminal or Basal identity, respectively.

On the other hand, ZBED2 has been shown to inhibit STAT2 and dampen inflammation by direct competition with IRF1 for Interferon Responsive Element binding in the pancreas [55]. We therefore sought to determine if ZBED2 is involved in the downregulation of interferon signaling in bladder cancer, potentially through interfering with FOXA1-activated pathways. Intriguingly, ZBED2 expression in the TCGA-BLCA cohort positively correlated with interferon gamma associated gene expression (Fig. S8D), which could be an indication that ZBED2 increases in response to inflammation at the cell population level, or vice versa. We then examined the correlation between ZBED2 expression and different cellular pathways at the single-cell level using publicly available scRNA-seq data [36]. Our analysis revealed that ZBED2 expression anti-correlates with interferon response and positively correlates with cell cycle progression and *E2F* targets within the same cell (Fig. 7E), suggesting that the positive correlation with interferon response in the bulk RNA-seq data reflects increased levels of ZBED2 expression and interferon response genes in different subpopulations of cells. To test this association further, we knocked down ZBED2 by siRNA and performed bulk 3' RNA-seq in two BLCA cell lines. Strikingly, downregulation of ZBED2 increased expression of interferon response genes and decreased expression of cell cycle progression and *E2F* target genes (Fig. 7F). Furthermore, siZBED2 in both RT112 and SCaBER cells slightly increased gene expression of *STAT2* and *CD274* (Fig. 7G) and tended towards decreased cell viability (Fig. S8E). Therefore, ZBED2 could directly dampen interferon response in bladder cancer, in agreement with its reported role in the pancreas [55]. Notably, siRNA of *FOXA1*

induced strong *STAT2* and *CD274* expression, while double knock-down of both *FOXA1* and *ZBED2* partially dampened this response compared to siFOXA1 alone (Fig. 7G), suggesting that the inflammatory response resulting from FOXA1 knock-down is partially dependent on ZBED2 target genes. In conclusion, both FOXA1 and ZBED2 inhibit inflammatory response and promote bladder cancer cell survival.

DISCUSSION

Epigenetic mechanisms are essential for the establishment and maintenance of cellular identity notably through enhancer regulation of master transcriptional regulators [17]. Bladder cancer has been extensively studied at the transcriptomic level, but until two recent studies, very little was known about its epigenetic landscape [27, 28].

Here, we report a large epigenetic profiling of both bladder cancer primary tumours and bladder cancer cell lines representative of the main molecular subtypes, as well as NHU cultures, using three histone marks ChIP-seq and paired RNA-seq. Using integrative analyses of all chromatin marks, we established to our knowledge the first comprehensive chromatin state map of bladder cancer using ChromHMM, and showed that Basal and Luminal subgroups can be distinguished by their chromatin profiles. This map can be used to identify new genes or regulatory regions for diagnostic, prognostic or pharmacological targeting.

We characterized the bladder SE repertoire, and through differential analysis identified subgroup-specific and cancer-specific SE activation.

Consistent with the two recently reported enhancer landscapes of bladder cancer [27, 28], Luminal-activated SE were located in proximity to known key regulators of the Luminal phenotype, namely *FOXA1*, *GATA3*, and *PPARG* [3, 14, 28], and to new Luminal-associated genes, such as *NPAS2* and *GRHL2* – also identified by Iyanki et al. [27] – or *KLF5*, recently characterized as activated through super-enhancer amplification in various squamous cell carcinomas [43]. Importantly, based on our data for 7 Ba/Sq samples, we were able to identify higher enhancer activity associated with potential key genes in Basal tumour biology, including cell surface receptors (*IL7R*, *OSMR*, *EGFR*, *MET*) and transcriptional regulators (*BNC2*, *HMG2*, *KLF7*, *NR3C1*).

In the previous publications (refs. [27, 28]), TF binding motif analysis in enhancer regions was applied to identify subtype-specific transcriptional regulators. Here, we further characterized subgroup-associated master regulators and co-regulated networks for both Luminal and Ba/Sq subgroups using two complementary approaches, in order to overcome issues linked to low expression, unknown binding motifs or multi-partner complexes. First, we identified TFs with enriched binding sites or DNA motifs in subgroup-specific enhancers. Second, we combined SE activity in our cohort with regulon analysis of TCGA data to identify master regulator networks for Luminal and Basal subgroups. The first approach, based on public ChIP-seq data, validated the role of TFs involved in urothelial differentiation in Luminal SE activity, namely FOXA1 and GATA3, but also revealed that the AP-1 complex

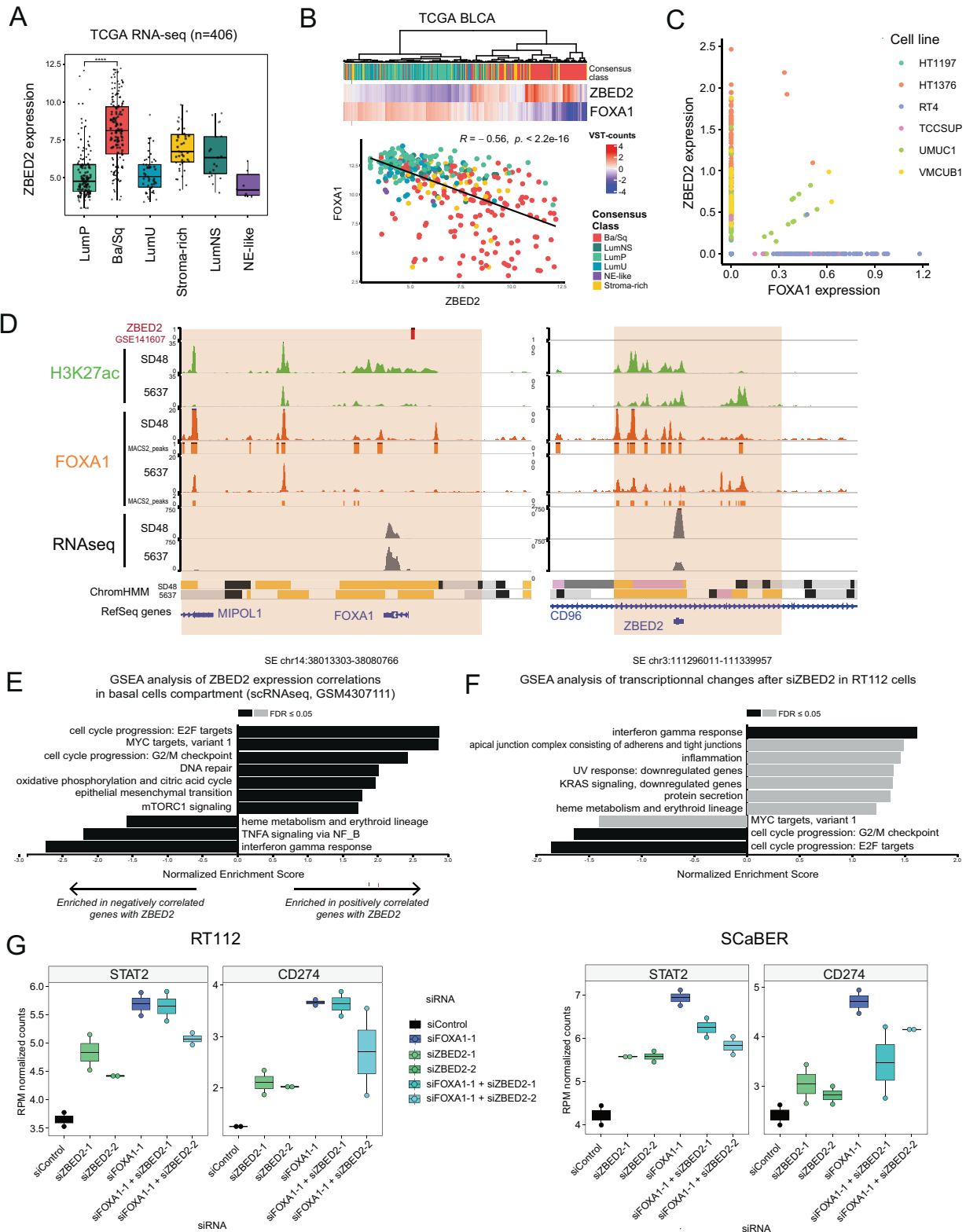


Fig. 7 ZBED2, a novel Basal-associated TF also involved inflammation dampening. **A** TCGA expression of ZBED2 by Subtypes. **B** TCGA expression Heatmap of ZBED2 and FOXA1 and TCGA correlation between ZBED2 and FOXA1. **C** Expression of FOXA1 and ZBED2 in single-cell transcriptomics from bladder cancer cell lines in the Cancer Cell Line Encyclopedia (CCLE), highlighting the nearly mutually exclusive expression of these genes. **D** Genome browser view of ZBED2 and FOXA1 loci in SD48 and 5637 cell lines. **E** GSEA analysis (Hallmark) of ZBED2 correlated genes in basal cells population of GSM4307111 scRNA-seq Tumour. **F** GSEA analysis (Hallmark) of gene expression upon siZBED2 KD in RT112 (siZBED2-1 and siZBED2-2). **G** 3' seq STAT2 and CD274 (PD-L1) expression in RT112 and SCaBER after siZBED2 and siFOXA1.

regulates Basal SEs. AP-1 has been shown to drive reprogramming of breast cancer cells from a Luminal to a Basal phenotype during treatment resistance acquisition through high-order assemblies of transcription factors [59]. Thus, a role for AP-1 in driving Basal enhancers and cell identity in bladder cancer suggests AP-1 inhibitors as potential therapeutic options for this aggressive disease. Interestingly, our mapping of FOXA1 binding sites in two different cell models indicated that the pioneer factor binds most bladder-associated enhancers, even if its DNA binding motif is mostly found in the Luminal-specific SEs. The mapping of FOXA1 binding also confirmed that FOXA1 binding sites in Basal enhancers are associated with AP-1 localization, suggesting that AP-1 could play an important role in the regulation of Basal regulatory regions through FOXA1 recruitment—or trapping—at discrete chromatin loci. By combining the ChIP-seq approach with regulon analysis, we were able to highlight new Luminal-associated TFs, in addition to known Luminal master regulators (FOXA1, GATA3, PPARG) and the recently identified NPAS2 [27]. Importantly, we also identified a Basal TF network, including ZBED2, KLF7, HMGA2, and NR3C1 as major regulators, whose expression was restricted to the basal component of tumours, according to scRNA-seq data. To our knowledge, the role of these TFs has not been investigated in bladder cancer biology.

With regards to ZBED2, a scRNA-seq study revealed that it promotes basal cell identity of keratinocytes [54]. Another study demonstrated that in pancreatic cancer, ZBED2 represses differentiation and dampens STAT2-mediated inflammatory response through IRES binding competition with IRF1 [55].

Modulation of master regulators can induce cell identity switch and resistance to therapy [22, 59]. FOXA1 pioneer factor notably controls cell identity in multiple models, during development and through enhancer binding [58, 61–63]. In particular, it has been shown in breast cancer cells that FOXA1 maintains luminal cell identity and controls plasticity between basal and luminal cells, not only by promoting the ER-dependent transcriptional program, but also by recruiting repressors to inhibit the expression of Triple Negative/Basal genes [64]. Previous work showed that the three master Luminal TFs (FOXA1, GATA3, and PPARG) had to be perturbed simultaneously to induce a cell identity switch from luminal to basal in bladder cancer cell lines [14]. However, we found that while short term knock-down of FOXA1 had a mild effect on cell identity, the long-term inactivation of FOXA1 alone through CRISPR mutation was sufficient to induce a shift from Luminal to Basal subgroup in luminal cells, highlighting the role of FOXA1 in the regulation of cell fate. Moreover, we demonstrated that this major shift is accompanied by activation of one of our newly identified Basal network TFs, ZBED2. Despite its known role as an activator of transcription, FOXA1 has also been associated to direct repression of transcription [65]. ZBED2 is described as a transcriptional repressor [55]. Therefore, FOXA1 and ZBED2 could repress each other, defining a new cell identity regulatory loop. Through functional knock-down and knock-out experiments, we verified that FOXA1 and ZBED2 have antagonistic but interconnected functions in cell identity. However, ZBED2 is expressed at a very low level and additional experiments, including overexpression models are needed to validate its repressive function on FOXA1, or vice versa, and its potential role in Luminal to Basal plasticity.

Finally, our work also uncovers a role for both FOXA1 and ZBED2 in the regulation of inflammation in bladder cancer. While they play antagonistic roles in the regulation of cell identity, we found that they share a common function in inhibiting inflammation. Short term loss of either FOXA1 or ZBED2 triggers an inflammatory response, identified through STAT2 overexpression, in agreement with the study of ZBED2 function in the pancreas [55]. The low FOXA1 binding enrichment at STAT2 in our FOXA1 ChIP-Seq experiments suggest that FOXA1 could have a repressive function of inflammation presumably independent of its chromatin binding. These conclusions are in accordance with the recent work of He

et al. [60] characterizing a chromatin independent function of FOXA1, which, by direct binding of STAT2 protein, inhibited STAT2-mediated inflammation. This could explain the limited infiltrate of luminal tumours, expressing high levels of FOXA1.

Therefore, given the dual role of FOXA1 and ZBED2 in the regulation of cell identity and inflammation, it will be important to study their link with tumour plasticity and in response to immunotherapy. Although direct inhibitors do not yet exist, targeting FOXA1/ZBED2 or the upstream or downstream signaling pathways, may improve sensitivity to immune-based therapies. Similarly, it will be worth studying the effect of interferon treatment on FOXA1 and ZBED2 inhibited inflammation as it could be used to overcome the inflammation inhibition induced by these two master regulators.

If FOXA1 and ZBED2 revealed promising features, our study identified numerous other super enhancers, associated genes and master regulators that could be explored for pharmacological targeting.

General targeting of SEs with BRD4 inhibitors has shown efficiency, in particular in cancers with specific SE single mutation alterations or with the activation of MYC SE in leukemia or lymphoma [15, 21, 66]. However, those treatments show mild efficiency in solid tumours and enhancer rewiring has been associated to resistance to treatment. Identification of major enhancers associated with bladder cancer and subgroups may pave the way for further research into targeting activated master regulators, upstream/downstream activated pathways or even with the advent of RNA and CRISPR technology, directly targeting enhancers.

CONCLUSIONS

We provide an integrated epigenomic and transcriptomic map of bladder cancer constituting a new comprehensive tool to study epigenetic regulation of muscle-invasive bladder cancer. We revealed Luminal and Basal coregulated networks of super-enhancers and associated transcription factors as new potential targets with important clinical relevance. Our findings and functional assays on FOXA1 and ZBED2 demonstrate that the enhancer set and TF networks identified herein represent prime targets for further pre-clinical investigation for bladder cancer treatment.

MATERIAL AND METHODS

Cell lines and culture

The human bladder cancer-derived cell lines RT112, 5637, KK47, and SCaBER were obtained from DSMZ (Heidelberg, Germany). MGH-U3, KK47 and SD48 cell lines were provided by Yves Fradet (CRC, Quebec), Jennifer Southgate laboratory (previously of Cancer Research Unit, St James's University Hospital, Leeds, UK), and Henri Mondor Hospital (Créteil, France), respectively. The L1207 cell line was derived from tumour T1207 [67]. RT112 and 5637 cells were cultured in RPMI medium, L1207 were cultured in DMEM-F12 and all the other cell lines were cultured in DMEM medium. All cell media were supplemented with 10% fetal bovine serum (FBS). We used Normal human urothelium (NHU) cells obtained from normal ureter urothelium from healthy kidney donors from Foch hospital and were cultured as previously described [68]. NHU derived from ureter have been shown to be transcriptionally very similar to NHU derived from bladder [69, 70]. All cells were cultured at 37 °C in an atmosphere of 5% CO₂ and were routinely tested for mycoplasma contamination.

Patient tumours

Tumours used in this study were previously characterized in our CIT (Carte d'Identité des Tumeurs) cohort [9, 29]. The characteristics of the tumours are shown in Table S1.

Resources

Antibodies, Vectors, Oligos, commercial assays and tools used in the study are detailed in the Supplemental information file.

Assignment of MIBC and NMIBC subtypes

Gene expression data of the most tumours cases was previously generated and published [9, 29]. We assigned consensus classes using the previously generated gene expression data using ConsensusMIBC (v1.1.0) R package [3] (Table S1). Given potential intra-tumour molecular heterogeneity, we also to verify the subtype in our ChIP-seq sampled tumour area using RNA-seq from the same powder using the same ConsensusMIBC (v1.1.0) R package.

NMIBC samples ($n = 2$) were classified using classifyNMIBC R Package [7].

Molecular-subtyping classification to BCa cell lines

We designed a tumour-reference similarity-based machine-learning driven approach to assigning molecular subtypes derived from BCa tumours to cell lines, to overcome the infeasibility of directly applying Tumour molecular-subtyping classifiers to cell lines due to intrinsic large difference in transcriptome profiles between the two different sample types. The idea is to measure the transcriptome similarity of the cells lines to a panel of reference tumours of different subgroups and calculate a probability score to each molecular subtype by k -nearest neighbors (KNN) classification in a number of randomly generated compressed feature spaces. The analysis involves a multi-step pipeline that covers data normalization, feature selection, data fusion with batch-effect correction, random compressed feature space generation, KNN-based classification, and subtype probability score calculation.

We applied the approach for molecular classification of BCa cell lines. We tested the robustness of the method using transcriptome data of 124 samples of 47 BCa cell lines profiled by two different transcriptome profiling method (mRNA-seq and Affymetrix HuST1.0 exon array) from four different sources, described as follows: 1. Cancer Cell Line Encyclopedia (CCLE) dataset, 36 cell lines with one sample for each, RNA-seq, downloaded from the DepMap Data Portal release19Q4, as transcripts per million normalized (TPM) counts; 2. MD Anderson (MDA), 30 cell lines with one sample for each, RNA-seq, downloaded from Gene Expression Omnibus with an accession GSE97768, as raw counts and then relative log-expression normalized (RLE); 3. In-house data of our lab team oncologie moleculaire (OM), 53 samples of 33 cell lines including xenografts (xeno), Affymetrix HuST1.0 exon array, robust multichip average (RMA) normalized; 4. In-house data of our lab team oncologie moleculaire (OM), 5 samples of 5 cell lines, RNA-seq, RLE normalized. The reference tumours for RNA-seq cell line samples were TCGA-BCa RNA-seq tumour transcriptomes ($n = 430$) and normalized in accordance with the cell line normalization, namely TPM for CCLE samples and RLE for MDA samples. The reference tumours for microarray samples were CIT MIBC tumours profiled with Affymetrix HuST1.0 exon array ($n = 160$), which were normalized with RMA. Our previous MIBC consensus molecular classification framework was applied to the reference tumour transcriptomes, and the NE-like and Stroma-rich subtypes were aggregated as 'double-negative'. The analyses were performed separately for each dataset. Briefly, the normalized cell line and reference tumour transcriptomes were first merged by taking the intersection of the transcriptome features. Then, the top 2000 genes with largest between-class variances among the reference tumours calculated by F -test were used as selected subtype-relevant features for subsequent analysis. One thousand 2-dimension tSNE embedding spaces were then generated using 1000 random-sequences. For each sample of the cell lines, KNN-based classification ($k = 6$) was performed in each tSNE embedding, and the predicted molecular class with the highest frequency was considered the molecular class for the cell line sample.

The predicted molecular subtypes were basically consistent across different profiling method and datasets and were coherent with prior knowledge. For example, the *FGFR3*-altered cell lines RT4, UMUC14, and SW780 were consistently classified as LumP subtype and the squamous BCa cell line SCaBER was consistently classified as Ba/Sq subtype, independent of dataset and profiling techniques. The *FGFR3*-altered RT112 cell line was basically classified as LumP across samples, with only one exception which was likely due to culturing or profiling artefact. In cell lines with samples classified as more than one subtypes, nearly all the cases were between Ba/Sq and double-negative subtypes. It was rare that the classifications were either luminal or basal for different samples of the same cell line (CAL29, UMUC6, and UMUC16). Regarding the 7 cell lines used for epigenomic profiling in the present work, the SD48, MGHU3, and RT112 were classified as the LumP subtype, and the SCaBER, L1207, and 5637 were classified as the Ba/Sq subtype, and the KK47 was classified as the double-negative subtype. No between-sample inconsistency was noted for these 7 cell lines (Table S1B, sheet 2).

Patient tumour tissue processing

We selected human tumours with an available OCT-compound frozen block from our CIT (Carte d'Identité des Tumeurs) cohort [9, 29]. Each block was frozen-sectioned and stained with hematoxylin and eosin. Pathology review was performed to confirm the tumour stage and to select tumour areas, in order to enhance neoplastic content (estimated at 30 to 95%, median tumour cell content = 65%). For tumours with sufficient material, tumour-enriched areas were macrodissected from the frozen block and manually finely ground in a mortar. Frozen ground tumour tissue was kept at -80°C until further processing.

Chromatin immunoprecipitation and sequencing

Tumour chromatin cross-linking and extraction. In order to obtain efficiently disrupted tissue, the frozen ground material (15 mg) was further homogenized using a tube pestle or the TissueLyser II system (Qiagen). Disrupted tissue was then processed using the reagents from the iDeal ChIP-seq Kit for Histones (Diagenode), according to the manufacturer's instructions. Briefly, the tissue was homogenized and washed in 1 ml PBS-protease inhibitor cocktail. DNA-protein cross-linking was ensured with an 8 min incubation in 1% formaldehyde then quenched with 0.125 M glycine for 5 min. Cells were then washed and lysed. Centrifuged cell lysates were resuspended in shearing buffer and sonicated using the Pico Bioruptor device (Diagenode) for 15 min (30 s ON/30 s OFF). Following a centrifugation at 16,000 g for 10 min, an aliquot was reserved to control the sonication and the remaining supernatant was stored at -80°C . Sonication efficiency was controlled for each sample on the aliquot of sheared chromatin by overnight reverse cross-linking, DNA was purified using the phenol-chloroform method and 2% agarose gel electrophoresis was used to determine DNA fragment size.

Tumour ChIP-seq. Tumour samples with optimal chromatin fragment size (200–500 bp) were immunoprecipitated using the iDeal ChIP-seq Kit for Histones (Diagenode). Magnetic immunoprecipitation of sheared DNA-chromatin complexes (500 ng) was performed overnight using a rabbit polyclonal histone H3K27acetyl ChIP Grade antibody (ab4729, Abcam), H3K27me3 (Active Motif, ref. 39155), and H3K9me3 (Active Motif, ref. 39161). Magnetic immunoprecipitation beads were washed the following day. The captured chromatin as well as non-immunoprecipitated input chromatin underwent elution and reverse cross-linking steps. DNA purification was performed using iPure magnetic beads. Immunoprecipitation (IP) efficiency was verified by qPCR according to the manufacturer's protocol using primers in positive region (GAPDH promoter) and negative regions. Library preparation from IP DNA and input DNA was performed using the Diagenode MicroPlex Library Preparation kit v2. The resulting amplified libraries were assessed using the Bioanalyzer system 2100 (Agilent) and sequenced using the HiSeq 4000 platform (Illumina) as single-read 50 base reads, following Illumina's instructions. Reads were aligned to the reference genome (Hg19) using Bowtie 1.0.0.

Cell line ChIP-seq. Cell lines cultures were crosslinked directly in the growing medium with formaldehyde 1% for 10 min at room temperature. The reaction was stopped by adding Glycine with a final concentration of 0.125 M for 10 min at room temperature. Fixed cells were rinsed 3 times with PBS containing protease inhibitors, pelleted, and resuspended in lysis buffer (10 mM EDTA, pH8, 50 mM Tris-HCl pH8, SDS 1%). After centrifugation, the ChIP was performed using ChIP-IT High Sensitivity kit (Active Motif, Carlsbad, CA, USA), following the manufacturer's instructions. Chromatin was sonicated in a bioruptor Pico device (Diagenode) for 10 min (30 s ON/30 s OFF). Sheared chromatin was immunoprecipitated using an H3K27ac antibody (Abcam ab4729). Sheared chromatin was used as input-DNA control.

ChIP-seq libraries were prepared using NEXTflex ChIP-Seq Kit (#5143-02, Bioo Scientific) following the manufacturer's protocol (V12.10) with some modifications. Briefly, 10 ng of ChIP enriched DNA were end-repaired using T4 DNA polymerase, Klenow DNA polymerase and T4 PNK, then size selected and cleaned-up using Agencourt AMPure XP beads (#A63881, Beckman). A single 'A' nucleotide was added to the 3' ends of the blunt DNA fragments with a Klenow fragment (3' to 5' exo minus). The ends of the DNA fragments were ligated to double stranded barcoded DNA adapters (NEXTflex ChIP-Seq Barcodes - 6, #514120, Bioo Scientific) using T4 DNA Ligase. The ligated products were enriched by PCR and cleaned-up using Agencourt AMPure XP beads. Prior to sequencing, DNA libraries were checked for quality and quantified using a 2100 Bioanalyzer (Agilent). The libraries were sequenced on the Illumina Hi-Seq 2500 as single-end 50

base reads following Illumina's instructions. Sequence reads were mapped to reference genome hg19 using Bowtie 1.0.0.

ChIP-seq data analysis and integration

Peak detection was performed using MACS2 (model-based analysis for ChIP-seq v2.1.0.20140616) software under settings where input samples were used as a negative control. We used a default cutoff and -B option for broad peaks for histone marks, and narrow peaks option for transcription factors. Firstly the bedGraph tracks for IP and Input samples were generated individually using macs2 callpeak (with option -SPMR-B). The IP signal was then compared with the corresponding Input signal using macs2 bdgcmp (with option -m FE). Finally, the bedGraph was converted to bigwig using the UCSC bedGraphToBigWig utility.

To identify enhancer regions in each tumour we used ROSE (Ranked Ordering of Super-Enhancers) algorithm [21, 41], with the following parameters: 12.5 kb stitching distance, exclusion of promoter regions 2500 bp around TSS. For each sample, stitched enhancer regions are normalized, ranked and plotted. The regions above the inflexion point are considered super-enhancers by the algorithm. However, the number of called super-enhancers was notably lower in cases with a known amplified gene. The very high H3K27ac signal in the amplified region likely created a bias in the plot of ranked enhancers. To correct for this bias, we selected from each sample ROSE output (AllEnhancers.table.txt ranked table) the top 1000 ROSE-ranked enhancers as candidate super-enhancer regions.

Heatmaps and PCA of ChIP-seq signal were performed using Diffbind R package (version 2.16.0) or Eseq [71]. For super-enhancers analysis, the top 1000 SE regions of either tumours or cell lines were merged for a consensus using Diffbind. Then, H3K27ac signal was calculated in the consensus peak for each sample. Differential analysis between molecular subtypes was performed with Diffbind and DESeq2 default parameters using both IP and input bam files, and a file containing the consensus super enhancer regions evaluated for differential analysis as input. Regions with a p -value < 0.05 were considered differentially bound.

Genomic annotation and pathway enrichment analyses were performed using ChIPseeker, clusterProfiler and GREAT (28).

Chromatin binding enrichment analysis. Factor binding analyses were performed using public data available in Cistrome DB Toolkit [48, 49]. DNA binding motif analysis was performed using HOMER known motif function [50].

Genomic annotation of the SE regions and cis-regulatory genes. SE activity and gene expression was jointly analyzed to determine the cis-regulatory between the SEs and genes on proximity. In brief, genes corresponding to each SE were annotated using ROSE (ROSE_geneMapper.py, identifying overlapping and proximal genes), but also with GREAT using "Basal plus extension parameters", as the candidate proximal genes regulated by the SE [41, 72]. The spearman correlation coefficients between SE activity (H3K27ac read counts, log2RPKM normalized) and the expression of the candidate genes (RLE normalized) were calculated in the tumours. The gene whose expression showing the highest correlation with the activity of the corresponding SE was determined as the gene most likely regulated by the SE. The SE-gene relationships within the top 1% were also given, not limited to the proximal genes. The number of germline single nucleotide polymorphisms (SNPs) within a given SE as well as their association with bladder cancer (median $-\log_{10} p$ -value) was provided based on the UK biobank GWAS summary statistics (Neale lab Round 2, ukb-d-C67, extracted from the MRC IEU OpenGWAS database) [73]. The germline SNPs falling within the SEs and with published GWAS-level association with BCa or with $-\log_{10} p$ -value > 5 in GWAS summary statistics (PhenoScanner v2 database) were provided as GWAS SNPs within the SEs [74]. For the genes most likely regulated by a given SE, we provided their median CERES dependency score of all and urothelial cancer cells from the Cancer Dependency Map database [56], as well as the p -value for difference between the two. We checked if any bias compared to the background in mutation type (missense, non-sense, synonymous, etc.) for the protein coding genes by Chi-square test. We checked if they were within the list of established cancer genes, including the COSMIC Cancer Gene Census and Network of Cancer Genes 6 [75, 76].

Chromatin state analysis and correlation with expression. ChromHMM was used to identify chromatin states. The genome was analyzed at 1000 bp intervals and the tool was used to learn models from the 3 histone marks ChIP-seq reads files and corresponding Input controls. A model of 6 states

was selected and applied on all samples. The 6 states identified were then given functional annotation based on histone marks enrichment and ENCODE published chromatin states.

We checked the genome-wide association between gene expression and chromatin states of the TSS, in both tumour and cell line samples. In each tumour/cell line, we classified the genes according to the chromatin states of the TSS. For genes with multiple TSS, the chromatin states showing frequency dominance was considered. We then calculated the median expression of the genes by their TSS categories in each sample, and assessed the distribution of the median expression by chromatin state across all tumour and cell line samples.

ChromHMM output files were concatenated using the unionbed function from BEDTools, by which a consensus sample-by-states matrix was created, where in each cell the chromatin state corresponding to the column's chromosome region in the row's sample, excluding regions from sexual chromosomes, with all samples included ($n = 24$, including 15 tumours and 9 cell lines).

We next performed unsupervised analysis of the integrated chromatin states in tumour and cell line samples.

Selection of most informative features. We first looked for the most informative features in the consensus sample-by-states matrix where in each cell the chromatin state corresponding to the column's chromosome region in the row's sample, excluding regions from sexual chromosomes, with all samples included ($n = 24$, including 15 tumours and 9 cell lines). We excluded genome regions of 'no mark' state to enrich our feature selection with active regions and filtered features with top 1% Shannon's entropy. Then to further select informative feature, we signed-rank transformed the data: For each state, given the constitution of the histone marks and association with gene expression, we performed a numeric transformation of the categorical states by assigning numeric values to categorical states, as 3 to E2 (Active Enhancer / Promoter), -3 to E4 (Repressed Chromatin), 2 to E3 (Bivalent Enhancer / Promoter), -2 to E6 (Heterochromatin / ZNF/ Repeats), 1 to E1 (Quiescent / No mark), and -1 to E5 (Quiescent / Weak repression). This allow to further increased the selection power as the top 1% features by variance ranking. We then used these top 1% variable features for subsequent analysis.

Dimension reduction and functional ontology analysis. We performed dimension reduction and visualization taking directly the categorical format of the above described selected features using multiple correspondence analysis (MCA). To explore the biological significance of the regions that contributed to the dimension that distinguishes the non-basal and basal clusters, the chromosome segments' loading estimates to the Dim 2 were extracted from the MCA outputs and regions with a p -value < 0.05 for the loading estimate were included ($n = 12,198$). Genes mapped to Dim 2 contributing regions were pre-ranked by loading estimates for gene-set enrichment analysis (GSEA) by which we identified multiple biological gene sets / ontologies associated with Dim 2. The gene sets collections were retrieved from the Broad Institute Molecular Signature Database, spanning the H (hall mark gene sets), C2 (curated gene sets, e.g., pathways), C3 (regulatory target gene sets), C5 (ontology gene sets, e.g., Gene Ontology), C6 (oncogenic signature gene sets), and C8 (cell type signature gene sets) categories, using the msigdb R package [35, 77].

As complementary exploration, we in the meantime performed dimensional reduction to the numeric transformed data of the selected features, using MDS. Similar to what was observed in MCA, the Dim 2 represents the dimension that distinguishes the basal versus non-basal samples, and Dim 1 separates cell lines from tumours, suggesting potential batch effect and/or in vitro culture-specific effect. We then adjusted for these latent effects to obtain a refined clustering (basically on Dim 2), using the MNN algorithm implemented in the fastMNN function of the batchelor R Bioconductor package [78].

We then calculated for the chromosomal segments (i.e., features of the consensus sample-by-states matrix), the difference in the numeric chromatin state scores between basal and non-basal groups, named chromatin state score difference basal vs non-basal. A negative score difference indicates stronger activation in the non-basal group, and a positive one indicates stronger activation in the basal group. For subsequent function analysis, we performed expression quantitative trait locus (eQTL) mapping to refine the segments to the ones significantly linked with associated gene expression, and limited the analysis to the significant eQTL pairs (p -value < 0.05, $n = 4377$). We then analyzed the distribution of the chromatin state score difference of the segments corresponding to the luminal and basal cell type signature genes.

RNA extraction and sequencing

Tumour RNA sequencing. Tumour RNA was extracted as described in refs. [72, 79].

RNA sequencing libraries: Kit Nugen. The pool of libraries was quantified using a qPCR method (KAPA library quantification kit, Roche). The sequencing was carried out using paired-end mode (PE100) on an Illumina Novaseq 6000 instrument, using a custom primer (provided into the Nugen kit) to initiate the Read 1 sequencing. The target number of reads was about 50 million paired-reads per sample.

Cell line RNA sequencing. Cell line RNA was extracted using Qiagen RNeasy kit coupled with DNase treatment. RNA sequencing libraries were prepared from 1 µg of total RNA using the Illumina TruSeq Stranded mRNA Library preparation kit (Illumina) which allows to perform a strand specific RNA sequencing. A first step of polyA selection using magnetic beads is done to focus sequencing on polyadenylated transcripts. After fragmentation, cDNA synthesis was performed and resulting fragments were used for dA-tailing and then ligated to the TruSeq indexed adapters. PCR amplification was finally achieved to create the final cDNA library (12 cycles). The resulting barcoded libraries were then equimolarly pooled and quantified using a qPCR method (KAPA library quantification kit, Roche). The sequencing was carried out using paired-end mode (PE100) on an Illumina HiSeq2000 instrument. The sequencing configuration was set to reach an average of 100 million paired-reads per sample.

Cell line 3'RNA-seq (Lexogen 3'Seq). RNA sequencing libraries were prepared from 200 ng of total RNA using the QuantSeq FWD 3'mRNA Seq LEXOGEN Standard (CliniSciences). Libraries were prepared according to the manufacturer's recommendations. The first step enables the synthesis of double strand cDNA, by revers transcription, using oligo dT priming. A qPCR optimization step was performed in order to estimate the most appropriate number of PCR cycles for library amplification. The resulting amplified and barcoded libraries were then equimolarly pooled and quantified using a qPCR method (KAPA library quantification kit, Roche). The sequencing was carried out using single-read mode (SR100) on an Illumina Novaseq 6000 instrument. The sequencing configuration was set to reach an average of 10 million reads per sample.

RNA-seq analysis

RNA-seq reads were aligned on genome hg19 using STAR with default parameters. Our RNA-seq as well as RNA-seq from public data repository (MGHU3 RNA-seq bulk data, GSE171129) were integrated using Deseq2 default parameters and VST normalization. 3'RNA-seq were analyzed with Deseq2 and RPM normalization.

Regulons

The regulatory network was reverse engineered by ARACNe-AP [53] from human urothelial cancer tissue datasets profiled by RNA-seq from TCGA. ARACNe was run with 100 bootstrap iterations using all probe-clusters mapping to a set of 1,740 transcription factors. Parameters used were standard parameters, with Mutual Information *p*-value threshold of 10^{-8} .

The VIPER (Virtual Inference of Protein-activity by Enriched Regulon analysis) [52] (R package vipier 1.24), using the regulatory network obtained from ARACNE on urothelial cancer, and we computed the enrichment of each regulon on the gene expression signature using different implementations of the analytic Rank-based Enrichment Analysis algorithm.

SE correlation network

To build SE driven correlation network, we first selected genes regulated by SEs defined as TFs in Lambert et al. [51]. Next using TCGA regulon VIPER score, we calculated the mean regulon score by subtype (Luminal, Ba/Sq or Stroma-Rich and kept TFs with mean regulon > 2 or < -2 ($n = 75$). We further restricted the list to TFs with a minimum expression correlation of 0.5 in TCGA to build correlation network using igraph.

Cell proliferation and Soft agar assays

For cell proliferation assays, cells were siRNA reverse transfected with Lipofectamine RNAi max in 6 well plate. Every 24 h post transfection and during 4 days, cells were counted using Malassez. Cells were then plated in soft agar and fixed after 21 days.

Cell treatments, cell viability assay

For siRNA treatments, cells were reverse transfected using Lipofectamine RNAi max (Invitrogen) using 10 ng of siRNA.

For CRispR mutant cell lines production, RT112 and SD48 cells were plated at 80% confluence and the day after transfected with vectors expressing Cas9 an gRNA (VectorBuilder) using Eugene HD transfection reagent. 48 h post transfection, cells were selected using Puromycin (2 µg/µL) during 4 days. After 2 weeks, clonal selection was performed using clonal dilution. FOXA1 mutation was assessed by Western Blot (anti-FOXA1 Abcam ab23738), PCR and genomic DNA sequencing.

For HA-FOXA1 overexpression, cells were plated at 80% confluence and the day after transfected with empty vector (pEmpty) or a vector expressing tagged FOXA1 (pHA-FOXA1). 48 h post transfection, cells were trypsinized and plated in media supplemented with Puromycin (2 µg/µL) for 24 more hours before RNA extraction.

Cell Viability was assessed in 96 well plates using CellTiter-Glo® Luminescent Cell Viability Assay (Promega). siRNA and CrispR vectors used in the study are referenced in the Supplementary information file.

RT-qPCR

Reverse transcription was performed using RT Applied high capacity kit. qPCR was performed on a Lightcycler 480 using SYBR or Probe Master as instructed by the manufacturer.

Immunohistochemistry

We performed a multiplex IHC staining combining 2 subtype markers: the luminal marker GATA3 (L50-823, Diagnostics), the basal marker CK5/6 (EP24/EP67, Diagnostics). Single stainings were performed for p16 (IHC116, Diagnostics), CK20 (Ks20.8, Dako). All IHC assays were performed on an automated stainer.

Public data

TCGA-BLCA MIBC RNA-seq data were downloaded from TCGA data portal using TCGAAbiolinks package (R), raw counts were normalized to account for different library size and the variance was stabilized with VST function in the DESeq2 R-package [80]. TCGA-BLCA samples ($n = 404$) were classified using the consensus system using consensusMIBC R package.

CLE urinary tract cell line gene expression was downloaded from the DepMap portal (<https://depmap.org/portal/download/>).

MGHU3 RNA-seq bulk data (GSE171129) as well as scRNA-seq from a Ba/Sq MIBC tumour (GSM4307111 [36]), were downloaded from GEO database.

Public scRNA-seq and Basal/Luminal signature

We downloaded the log2 TPM normalized gene expression of single cells from a Ba/Sq subtype MIBC tumour from the GEO database (accession number, GSM4307111 [36]). Initial quality control excluded genes expressed in less than 3 cells and cells with less than 200 genes. The top 2000 variable genes were used as features for subsequent PCA and the first 9 principal components were used for cell clustering and visualization by uniform manifold approximation and projection (UMAP) embedding. The marker genes of the luminal and basal tumour cells were calculated with Wilcoxon test-based approach. The single cell RNA-seq data analyses were performed using the Seurat v4 package with default parameters unless otherwise specified.

Given the single-cell derived luminal and basal tumour cell signature was based on single-cell sequencing of primary in vivo tumour sample, and the FOXA1 knock-out perturbation signature is likely limited to the genes regulated by FOXA1 in an in vitro setting, it is important to adopt the cell subtype signatures to refine to the marker genes regulated by FOXA1, as a FOXA1-dependent luminal-basal plasticity signature which could be then used for further analyses involving in vitro transcriptomes. We first compared the perturbation and single-cell signatures by GSEA (perturbation DEG effect for ranking, and luminal / basal signatures as gene sets of interest) and found that in RT112 cell line, there was both significant enrichment of luminal signature in genes down-regulated in FOXA1 KO clones and significant enrichment of basal signature in genes up-regulated in FOXA1 KO clones. We then took the leading edge genes as the adopted FOXA1-dependent plasticity signature. As validation, this adopted signature showed similar enrichment in RT112 FOXA1 KD assays and SD48 FOXA1 KO assays, while the original cell type signature failed.

General bioinformatics, statistical analyses

Plots and statistical analyses were performed in R software version 3.6.1, using ggpubr package, or Graphpad prism. Wilcoxon and Kruskal-Wallis tests were used to test the association between continuous and categorical variables, for 2 categories or > 2 categories, respectively. *P*-values < 0.05 were considered statistically significant. Pairwise correlation of gene expression was calculated using Pearson coefficient. All gene expression heatmaps show mean-centered log₂-transformed normalized counts of each represented gene. Heatmaps were produced using complexHeatmap or pheatmap.

Survival analysis

For Kaplan Meier survival analyses testing the association of gene expression and overall survival, we used <http://tumoursurvival.org/index.html> tool and divided the samples based on mean +/− sd. Log-rank *P* values were calculated to test the association between overall survival and low vs high expression groups.

DATA AVAILABILITY

The datasets supporting the conclusions of this article are available in the GEO repository under accession numbers: GSE193889 for Tumours ChIP-seq GSE193886 for Normal and Cancer cell culture ChIP-seq GSE195768 for Tumours RNAseq GSE195608 for Normal and Cancer cell culture RNA-seq GSE196595 for functional assays 3'RNA-seq This paper analyzes existing, publicly available data: GSE141606 (ZBED2 ChIP-seq), GSE141605 (ZBED2 Overexpression in PDA cell lines), GSM4307111 (scRNAseq Tumor public data), CCLE (<https://depmap.org/portal/download/>) and TCGA (TCGA data portal).

REFERENCES

- Bray F, Ferlay J, Soerjomataram I, Siegel RL, Torre LA, Jemal A. Global cancer statistics 2018: GLOBOCAN estimates of incidence and mortality worldwide for 36 cancers in 185 countries. *CA Cancer J Clin.* 2018;68:394–424.
- Humphrey PA, Moch H, Cubilla AL, Ulbright TM, Reuter VE. The 2016 WHO classification of tumours of the urinary system and male genital organs—Part B: Prostate and bladder tumours. *Eur Urol.* 2016;70:106–19.
- Kamoun A, de Reyniès A, Allory Y, Sjö Dahl G, Robertson AG, Seiler R, et al. A consensus molecular classification of muscle-invasive bladder cancer [Formula presented]. *Eur Urol.* 2020;77:420–33.
- Marzouka NAD, Eriksson P, Rovira C, Liedberg F, Sjö Dahl G, Höglund M. A validation and extended description of the Lund taxonomy for urothelial carcinoma using the TCGA cohort. *Sci Rep.* 2018;8. <https://doi.org/10.1038/s41598-018-22126-x>.
- Choi W, Porten S, Kim S, Willis D, Plimack ER, Hoffman-Censits J, et al. Identification of distinct basal and luminal subtypes of muscle-invasive bladder cancer with different sensitivities to frontline chemotherapy. *Cancer Cell.* 2014;25:152–65.
- Rebouissou S, Héralut A, Letouzé E, Neuzillet Y, Laplanche A, Ofualuka K, et al. CDKN2A homozygous deletion is associated with muscle invasion in FGFR3-mutated urothelial bladder carcinoma. *J Pathol.* 2012;227:315–24.
- Lindskrog SV, Prip F, Lamy P, Taber A, Groeneveld CS, Birkenkamp-Demtröder K, et al. An integrated multi-omics analysis identifies prognostic molecular subtypes of non-muscle-invasive bladder cancer. *Nat Commun.* 2021;12. <https://doi.org/10.1038/s41467-021-22465-w>.
- Hedegaard J, Lamy P, Nordentoft I, Algaba F, Høyer S, Ulhøi BP, et al. Comprehensive transcriptional analysis of early-stage urothelial carcinoma. *Cancer Cell.* 2016;30:27–42.
- Rebouissou S, Bernard-Pierrot I, de Reyniès A, Lepage M-LL, Krucker C, Chapeaublanc E, et al. EGFR as a potential therapeutic target for a subset of muscle-invasive bladder cancers presenting a basal-like phenotype. *Sci Transl Med.* 2014;6:244ra91.
- Fishwick C, Higgins J, Percival-Alwyn L, Hustler A, Pearson J, Bastkowski S, et al. Hierarchy of transcription factors driving basal and luminal cell phenotypes in human urothelium. *Cell Death Differ.* 2017;24:809–18.
- Eriksson P, Aine M, Veerla S, Liedberg F, Sjö Dahl G, Höglund M. Molecular subtypes of urothelial carcinoma are defined by specific gene regulatory systems. *BMC Med Genomics* 2015;8. <https://doi.org/10.1186/s12920-015-0101-5>.
- Yamashita H, Kawasawa YI, Shuman L, Zheng Z, Tran T, Walter V, et al. Repression of transcription factor AP-2 alpha by PPARγ reveals a novel transcriptional circuit in basal-squamous bladder cancer. *Oncogenesis* 2019;8. <https://doi.org/10.1038/s41389-019-0178-3>.
- Karni-Schmidt O, Castillo-Martin M, HuaiShen T, Gladoun N, Domingo-Domenech J, Sanchez-Carbayo M, et al. Distinct expression profiles of p63 variants during urothelial development and bladder cancer progression. *Am J Pathol.* 2011;178:1350–60.
- Warrick JI, Walter V, Yamashita H, Chung E, Shuman L, Amponsa VO, et al. FOXA1, GATA3 and PPARγ Cooperate to drive luminal subtype in bladder cancer: A molecular analysis of established human cell lines. *Sci Rep.* 2016;6:1–15.
- Chapuy B, McKeown MR, Lin CY, Monti S, Roemer MGM, Qi J, et al. Discovery and characterization of super-enhancer-associated dependencies in diffuse large B cell lymphoma. *Cancer Cell.* 2013;24:777–90.
- Ott CJ, Federation AJ, Schwartz LS, Kasar S, Klitgaard JL, Lenci R, et al. Enhancer architecture and essential core regulatory circuitry of chronic lymphocytic leukemia. *Cancer Cell.* 2018;34:982–995.e7.
- Hnisz D, Abraham BJ, Lee TI, Lau A, Saint-André V, Sigova AA, et al. Super-enhancers in the control of cell identity and disease. *Cell.* 2013;155:934.
- Blobel GA, Higgs DR, Mitchell JA, Notani D, Young RA. Testing the super-enhancer concept. <https://doi.org/10.1038/s41576-021-00398-w>.
- Sengupta S, George RE. Super-enhancer-driven transcriptional dependencies in cancer. *Trends Cancer.* 2017;3:269–81.
- Niederriter AR, Varshney A, Parker SCJ, Martin DM. Super enhancers in cancers, complex disease, and developmental disorders. *Genes (Basel).* 2015;6:1183–200.
- Lovén J, Hoke HA, Lin CY, Lau A, Orlando DA, Vakoc CR, et al. Selective inhibition of tumor oncogenes by disruption of super-enhancers. *Cell.* 2013;153:320–34.
- Lomberk G, Blum Y, Nicolle R, Nair A, Gaonkar KS, Marisa L, et al. Distinct epigenetic landscapes underlie the pathobiology of pancreatic cancer subtypes. *Nat Commun.* 2018;9:1978.
- Boeva V, Louis-Brennetot C, Peltier A, Durand S, Pierre-Eugène C, Raynal V, et al. Heterogeneity of neuroblastoma cell identity defined by transcriptional circuitries. *Nat Genet.* 2017;49:1408–13.
- Ooi WF, Xing M, Xu C, Yao X, Ramlee MK, Lim MC, et al. Epigenomic profiling of primary gastric adenocarcinoma reveals super-enhancer heterogeneity. *Nat Commun.* 2016;7:1–17.
- Ho SWT, Sheng T, Xing M, Ooi WF, Xu C, Sundar R, et al. Regulatory enhancer profiling of mesenchymal-type gastric cancer reveals subtype-specific epigenomic landscapes and targetable vulnerabilities. *Gut.* 2023;72:226–41.
- Dunham I, Kundaje A, Aldred SF, Collins PJ, Davis CA, Doyle F, et al. An integrated encyclopedia of DNA elements in the human genome. *Nature.* 2012;489:57–74.
- Iyanki T, Zhang B, Wang Q, Hou Y, Jin Q, Xu J, et al. Subtype-associated epigenomic landscape and 3D genome structure in bladder cancer. *Genome Biol.* 2021;22:2020.02.26.966697.
- van der Vos KE, Vis DJ, Nevedomskaya E, Kim Y, Choi W, McConkey D, et al. Epigenetic profiling demarcates molecular subtypes of muscle-invasive bladder cancer. *Sci Rep.* 2020;10:1–10.
- Biton A, Bernard-Pierrot I, Lou Y, Krucker C, Chapeaublanc E, Rubio-Pérez C, et al. Independent component analysis uncovers the landscape of the bladder tumor transcriptome and reveals insights into luminal and basal subtypes. *Cell Rep.* 2014;9:1235–45.
- Shi MJ, Meng XY, Fontugne J, Chen CL, Radvanyi F, Bernard-Pierrot I. Identification of new driver and passenger mutations within APOBEC-induced hotspot mutations in bladder cancer. *Genome Med.* 2020;12:85.
- Blum Y, Meiller C, Quétel L, Elarouci N, Ayadi M, Tashtanbaeva D, et al. Dissecting heterogeneity in malignant pleural mesothelioma through histo-molecular gradients for clinical applications. *Nat Commun.* 2019;10:1–12.
- Sjö Dahl G, Eriksson P, Liedberg F, Höglund M. Molecular classification of urothelial carcinoma: global mRNA classification versus tumour-cell phenotype classification. *J Pathol.* 2017;242:113–25.
- Ernst J, Kellis M. ChromHMM: Automating chromatin-state discovery and characterization. *Nat Methods* 2012;9:215–6.
- Mootha VK, Lindgren CM, Eriksson KF, Subramanian A, Sihag S, Lehar J, et al. PGC-1α-responsive genes involved in oxidative phosphorylation are coordinately downregulated in human diabetes. *Nat Genet.* 2003;34:267–73.
- Subramanian A, Tamayo P, Mootha VK, Mukherjee S, Ebert BL, Gillette MA, et al. Gene set enrichment analysis: A knowledge-based approach for interpreting genome-wide expression profiles. 2005 <https://doi.org/10.1073/pnas.0506580102>.
- Lee HW, Chung W, Lee H-O, Jeong DE, Jo A, Lim JE, et al. Single-cell RNA sequencing reveals the tumor microenvironment and facilitates strategic choices to circumvent treatment failure in a chemorefractory bladder cancer patient. <https://doi.org/10.1186/s13073-020-00741-6>.
- Parolia A, Cieslik M, Chu S-CC, Xiao L, Ouchi T, Zhang Y, et al. Distinct structural classes of activating FOXA1 alterations in advanced prostate cancer. *Nature.* 2019;571:413–8.
- Kim E, Choi S, Kang B, Kong JH, Kim Y, Yoon WH, et al. Creation of bladder assembloids mimicking tissue regeneration and cancer. *Nature.* 2020;588:664–9.
- Choi W, Czerniak B, Ochoa A, Su X, Siefker-Radtke A, Dinney C, et al. Intrinsic basal and luminal subtypes of muscle-invasive bladder cancer. *Nat Rev Urol.* 2014;11:400–10.

40. Robertson AG, Kim J, Al-Ahmadie H, Bellmunt J, Guo G, Cherniack AD, et al. Comprehensive molecular characterization of muscle-invasive bladder cancer. *Cell*. 2017;171:540–556.e25.
41. Whyte WA, Orlando DA, Hnisz D, Abraham BJ, Lin CY, Kagey MH, et al. Master transcription factors and mediator establish super-enhancers at key cell identity genes. *Cell*. 2013;153:307–19.
42. Aldiri I, Xu B, Wang L, Chen X, Hiler D, Griffiths L, et al. The dynamic epigenetic landscape of the retina during development, reprogramming, and tumorigenesis. *Neuron*. 2017;94:550–568.e10.
43. Zhang X, Choi PS, Francis JM, Gao GF, Campbell JD, Ramachandran A, et al. Somatic superenhancer duplications and hotspot mutations lead to oncogenic activation of the KLF5 transcription factor. *Cancer Disco*. 2018;8:108–25.
44. Weinstein JN, Akbani R, Broom BM, Wang W, Verhaak RGWW, McConkey D, et al. Comprehensive molecular characterization of urothelial bladder carcinoma. *Nature*. 2014;507:315–22.
45. Sim WJ, Iyengar PV, Lama D, Lui SKL, Ng HC, Haviv-Shapira L, et al. c-Met activation leads to the establishment of a TGF β -receptor regulatory network in bladder cancer progression. *Nat Commun*. 2019;10. <https://doi.org/10.1038/s41467-019-12241-2>.
46. Chen L, Huang M, Plummer J, Pan J, Jiang YY, Yang Q, et al. Master transcription factors form interconnected circuitry and orchestrate transcriptional networks in oesophageal adenocarcinoma. *Gut*. 2020;69:630–40.
47. Saint-André V, Federation AJ, Lin CY, Abraham BJ, Reddy J, Lee TI, et al. Models of human core transcriptional regulatory circuitries. *Genome Res*. 2016;26:385–96.
48. Zheng R, Wan C, Mei S, Qin Q, Wu Q, Sun H, et al. Cistrome Data Browser: Expanded datasets and new tools for gene regulatory analysis. *Nucleic Acids Res*. 2019;47:D729–D735.
49. Mei S, Qin Q, Wu Q, Sun H, Zheng R, Zang C, et al. Cistrome data browser: A data portal for ChIP-Seq and chromatin accessibility data in human and mouse. *Nucleic Acids Res*. 2017;45:D658–D662.
50. Heinz S, Benner C, Spann N, Bertolino E, Lin YC, Laslo P, et al. Simple combinations of lineage-determining transcription factors prime cis-regulatory elements required for macrophage and B cell identities. *Mol Cell*. 2010;38:576–89.
51. Lambert SA, Jolma A, Campitelli LF, Das PK, Yin Y, Albu M, et al. The human transcription factors. *Cell*. 2018;172:650–65.
52. Alvarez MJ, Shen Y, Giorgi FM, Lachmann A, Ding BB, Hilda Ye B, et al. Functional characterization of somatic mutations in cancer using network-based inference of protein activity. *Nat Genet*. 2016;48:838–47.
53. Lachmann A, Giorgi FM, Lopez G, Califano A. ARACNe-AP: Gene network reverse engineering through adaptive partitioning inference of mutual information. *Bioinformatics*. 2016;32:2233–5.
54. Finnegan A, Cho RJ, Luu A, Harirchian P, Lee J, Cheng JB, et al. Single-cell transcriptomics reveals spatial and temporal turnover of keratinocyte differentiation regulators. *Front Genet*. 2019;10:1–14.
55. Somerville TDD, Xu Y, Wu XS, Maia-Silva D, Hur SK, De Almeida LMN, et al. ZBED2 is an antagonist of interferon regulatory factor 1 and modifies cell identity in pancreatic cancer. *Proc Natl Acad Sci USA*. 2020;117. <https://doi.org/10.1073/pnas.1921484117>.
56. Barretina J, Caponigro G, Stransky N, Venkatesan K, Margolin AA, Kim S, et al. The Cancer Cell Line Encyclopedia enables predictive modelling of anticancer drug sensitivity. *Nature*. 2012;483:603–7.
57. Ghandi M, Huang FW, Jané-Valbuena J, Kryukov GV, Lo CC, McDonald ER, et al. Next-generation characterization of the cancer cell line encyclopedia. *Nature*. 2019;569:503–8.
58. Iwafuchi-doi M, Donahue G, Kakumanu A, Watts JA, Mahony S, Pugh BF, et al. The pioneer transcription factor FoxA maintains an accessible nucleosome configuration at enhancers for tissue-specific gene activation. *Mol Cell*. 2016;62:79–91.
59. Bi M, Zhang Z, Jiang YZ, Xue P, Wang H, Lai Z, et al. Enhancer reprogramming driven by high-order assemblies of transcription factors promotes phenotypic plasticity and breast cancer endocrine resistance. *Nat Cell Biol*. 2020;22:701–15.
60. He Y, Wang LLLL, Wei T, Xiao Y-TT, Sheng H, Su H et al. FOXA1 overexpression suppresses interferon signaling and immune response in cancer. *J Clin Invest*. 2021;131. <https://doi.org/10.1172/JCI147025>.
61. Roe JS, Hwang CI, Somerville TDD, Milazzo JP, Lee EJ, Da Silva B, et al. Enhancer reprogramming promotes pancreatic cancer metastasis. *Cell*. 2017;170:875–888.e20.
62. Camolotto SA, Pattabiraman S, Mosbrugger TL, Jones A, Belova VK, Orstad G, et al. FoxA1 and FoxA2 drive gastric differentiation and suppress squamous identity in NKX2-1-negative lung cancer. *Elife* 2018;7. <https://doi.org/10.7554/eLife.38579>.
63. Geusz RJ, Wang A, Lam DK, Vincikier NK, Alysandratos KD, Roberts DA, et al. Sequence logic at enhancers governs a dual mechanism of endodermal organ fate induction by FOXA pioneer factors. *Nat Commun*. 2021;12. <https://doi.org/10.1038/s41467-021-26950-0>.
64. Bernardo GM, Bebek G, Ginther CL, Sizemore ST, Lozada KL, Miedler JD, et al. FOXA1 represses the molecular phenotype of basal breast cancer cells. *Oncogene*. 2013;32:554–63.
65. Song B, Park SH, Zhao JC, Fong KW, Li S, Lee Y, et al. Targeting FOXA1-mediated repression of TGF β signaling suppresses castration-resistant prostate cancer progression. *J Clin Invest*. 2019;129:569–82.
66. Mansour MR, Abraham BJ, Anders L, Gutierrez A, Durbin AD, Lawton L, et al. An oncogenic super-enhancer formed through somatic mutation of a noncoding intergenic element. *Science*. 2014;346:1373–7.
67. De Boer WT, Houtsmuller AB, Izadifar V, Muscatelli-Groux B, Van Der Kwast TH, Chopin DK. Expression and functions of EGF, FGF and TGF β -growth-factor family members and their receptors in invasive human transitional-cell-carcinoma cells. *Int J Cancer*. 1997;71:284–91.
68. Southgate J, Masters JRW, Trejdosiewicz LK. Culture of Human Urothelium. In: *Culture of Epithelial Cells*. John Wiley & Sons, Inc.: New York, USA, 2003, pp 381–99.
69. Böck M, Hinley J, Schmitt C, Wahlich T, Kramer S, Southgate J. Identification of ERF3 as an early transcriptional regulator of human urothelium. *Dev Biol*. 2014;386:321–30.
70. Hustler A, Eardley I, Hinley J, Pearson J, Wezel F, Radvanyi F, et al. Differential transcription factor expression by human epithelial cells of buccal and urothelial derivation. *Exp Cell Res*. 2018;369:284–94.
71. Lerdrup M, Johansen JV, Agrawal-Singh S, Hansen K. An interactive environment for agile analysis and visualization of ChIP-seq data. *Nat Struct Mol Biol*. 2016;23:349–57.
72. McLean CY, Bristor D, Hiller M, Clarke SL, Schaar BT, Lowe CB, et al. GREAT improves functional interpretation of cis-regulatory regions. *Nat Biotechnol*. 2010;28:495–501.
73. Elsworth B, Lyon M, Alexander T, Liu Y, Matthews P, Hallett J, et al. The MRC IEU OpenGWAS data infrastructure. <https://doi.org/10.1101/2020.08.10.244293>.
74. Kamat MA, Blackshaw JA, Young R, Surendran P, Burgess S, Danesh J, et al. Databases and ontologies PhenoScanner V2: an expanded tool for searching human genotype-phenotype associations. <https://doi.org/10.1093/bioinformatics/btz469>.
75. Tate JG, Bamford S, Jubb HC, Sondka Z, Beare DM, Bindal N, et al. COSMIC: The catalogue of somatic mutations in cancer. *Nucleic Acids Res*. 2019;47:D941–D947.
76. Sondka Z, Bamford S, Cole CG, Ward SA, Dunham I, Forbes SA. The COSMIC cancer gene census: Describing genetic dysfunction across all human cancers. *Nat Rev Cancer* 2018;18:696–705.
77. Liberzon A, Birger C, Thorvaldsdóttir H, Ghandi M, Mesirov JP, Tamayo P. The Molecular signatures database hallmark gene set collection. *Cell Syst*. 2015;1:417–25.
78. Haghverdi L, Lun ATL, Morgan MD, Marioni JC. Batch effects in single-cell RNA-sequencing data are corrected by matching mutual nearest neighbors. *Nat Biotechnol*. 2018;36:421–7.
79. Benhamou S, Bonastre J, Groussard K, Radvanyi F, Allory Y, Lebert T. A prospective multicenter study on bladder cancer: The COBLANCE cohort. *BMC Cancer* 2016;16. <https://doi.org/10.1186/s12885-016-2877-x>.
80. Love MI, Huber W, Anders S. Moderated estimation of fold change and dispersion for RNA-seq data with DESeq2. *Genome Biol*. 2014;15:550.

ACKNOWLEDGEMENTS

We thank the NGS platform of Institut Curie, directed by Sylvain Baulande.

AUTHOR CONTRIBUTIONS

HN-K, JF, performed the ChIP-seq and RNA-seq experiments. CK established the NHU primary cells cultures. YN and TL provided clinical insight for analysis of the CIT cohort. JF under YA supervision performed histo-pathological analysis, EG the macrodissection of the tumours, and VD performed IHC. AR under DG supervision optimized RNA sequencing of primary tumour samples. HNK performed the functional experiments, siRNA, CRISPR, cellular assays, with the help of LT. HN-K, X-YM, CG, JF, TY, LC, FD, EC carried out the bioinformatics analysis. In particular, HN-K analysed ChIP-seq data, performed ChromHMM integration, SE identification with JF, differential analysis, ontology/GSEA analysis, 3'RNA-seq analyses, and established coregulatory network with the help of JF, FD, and DJ. CG designed R scripts and participated to several analyses (GSVA, SE differential analysis, classifications). LC performed the regulon analysis. X-YM. analysed ChromHMM output, publicly available scRNA-seq, derived Basal/Luminal signature, 3'RNA-seq, performed GSEA analysis, optimized SE annotation. TY under ID supervision processed the ChIPseq data. EC processed RNA-seq data of cell lines and centralized the data for bioinformatics analyses. HN-K, JF, X-YM, CG, DJ, IB-P, FR wrote the manuscript. The study was conceived by HN-K, JF, and supervised by YA, IB-P, and FR. All authors gave critical insights and approved the final version for publication.

FUNDING

The work was supported by grants from Ligue Nationale Contre le Cancer: (HN-K, JF, CG, X-YM, LC, FD, CK, YA, FR, IB-P) as an associated team (Equipe labellisée), the “Carte d’Identité des Tumeurs” program initiated, developed and funded by Ligue Nationale Contre le Cancer, and a post-doctoral fellowship supporting HN-K. JF was supported by the Fondation ARC pour la recherche sur le cancer, LC by FRM (Fondation Recherche Médicale) and X-YM was supported by a fellowship from ITMO Cancer AVIESAN, within the framework of Cancer Plan. The work was also supported by a “PL-Bio” project funded by INCa (2016-146), the French Ministry of Education and Research, the CNRS, and the Institut Curie. ChIP-sequencing was performed by the GenomEast platform, a member of the ‘France Genomique’ consortium (ANR-10-INSB-0009).

COMPETING INTERESTS

The authors declare no competing interests.

ETHICAL APPROVAL

All patients provided written informed consent. All research in this study conformed to the principles of the Helsinki Declaration. All patients consent to participate.

ADDITIONAL INFORMATION

Supplementary information The online version contains supplementary material available at <https://doi.org/10.1038/s41388-023-02662-1>.

Correspondence and requests for materials should be addressed to H el ene Neyret-Kahn.

Reprints and permission information is available at <http://www.nature.com/reprints>

Publisher’s note Springer Nature remains neutral with regard to jurisdictional claims in published maps and institutional affiliations.



Open Access This article is licensed under a Creative Commons Attribution 4.0 International License, which permits use, sharing, adaptation, distribution and reproduction in any medium or format, as long as you give appropriate credit to the original author(s) and the source, provide a link to the Creative Commons license, and indicate if changes were made. The images or other third party material in this article are included in the article’s Creative Commons license, unless indicated otherwise in a credit line to the material. If material is not included in the article’s Creative Commons license and your intended use is not permitted by statutory regulation or exceeds the permitted use, you will need to obtain permission directly from the copyright holder. To view a copy of this license, visit <http://creativecommons.org/licenses/by/4.0/>.

  The Author(s) 2023